Chapter 3

One-dimensional nanostructure growth in PAA

The 1D nanostructure synthesis is of high interest in many domains, since a lot of new properties can be revealed at this scale of matter. Some inherent challenges are however intimately related to this synthesis, namely the organisation, the handling and the contacting (in the case of electrical applications) of these nanostructures. In this chapter, we will introduce a method commonly used to easily organize the 1D nanostructures, as well as to make their handling and contacting easier. This method is the confined growth in nanometric-size tubular templates, which parallel pores receive the nanostructures like a mold. In that purpose, it is planned to use Porous Anodic Alumina (PAA) templates, already studied in the first chapter. In a first part we will set out a general definition of 1D nanostructures, explain their potential (and promising) applications and sum up the most promising devices reported in the literature hitherto. Then a section will be devoted to an overview of different synthesis techniques (including the one we used in this work to grow SiNWs and CNTs) and to the theoretical description of some growth mechanisms. In the section after we will introduce our experimental set up and discuss our results, before concluding this chapter.

3.1 Definitions and potential applications

In the most general sense, the term "nanostructure" refers to any ensemble which at least one dimension is between 1 and 100 nm. Nowadays, advanced fabrication techniques allow to fabricate a wide variety of nanostructures, thus described as "artificial", but of course Nature hasn't waited for human beings to exhibit ultra-small structures, with complex features, and equipped with natural ultra-sophisticated functionalities. Indeed, molecules, viruses, proteins... are fully part of the family of the nanostructures, for their size is generally inferior to 100 nm. The control of chemistry and physics allowed to fabricate plenty of nanostructures (nanofibres, nanoparticles, nanorods, nanotubes, nanoshells, nanorings, nanowires...) that can be classified according to their shape. More precisely, they are often classified regarding the number of dimensions that belong

to the nanoscale. Thus, a structure having only one dimension below 100 nm can be named a 2D nanostructure; this is the case for every "nanosheets", which thickness is often a few nanometers. In an extreme and famous case, graphene is a 2D nanocrystal, which thickness is only one carbon atom. Then come 1D nanostructures, which are nanometric in two spatial dimensions. They are the well-known nanotubes, nanowires (formerly named nanowhiskers), but also nanofibres, nanorods... and are the heart of this thesis. Finally come the so-called 0D structures. They exhibit dimensions below 100 nm in all the spatial dimensions and are usually referred to as nanoparticles, nanospheres, nanoshells... One should also mention the quantum dots, which implementation in electronic devices, medicine or computing is a burning topic.

Let's now focus on the potentialities of the 1D nanostructures, in order to foresee the interest of studying their growth in this thesis.

3.2 One dimensional (1D) nanostructures growth

3.2.1 Synthesis methods

In this section, the main routes to fabricate 1D nanostructures reported so far in the literature will be presented. A special attention will be paid on the fabrication of SiNWs and CNTs, since they constitute potential candidates for the NW/NT-based FET fabrication. Some exhaustive reviews by Gösele's group [1], [2], Shao, Ma and Lee [3] for SiNWs, Hernandez-Velez [4] or Xia and Yang [5] report a wide variety of methods to build up 1D nanostructures. One can distinguish between the top-down and the bottom-up strategies, which are basically related to physics and chemistry, respectively, though the frontier is not that clear, especially when both are used at the same time.

Top-down techniques

The top-down approach consists in going as far as possible in the etching of a given material, starting from a bulk sample, so as to reach the nanometer scale. A combination of lithography and etching allows the fabrication of nanowires, a patterned mask acting as a sacrificial layer to define the nanowires during the subsequent etching. In particular, electron beam lithography (EBL) allows to define patterns down to the low nanometer scale (a few nm) and is therefore often used in the top-down approach [6], [7]. Reactive ion etching (RIE), which principle will be presented in chapter 4, is often used, for its high anisotropy can provide high aspect ratio structures. A subsequent wet etching can lead to suspended wires [8], [9]. These last two references utilize a very commonly-used technique to decrease the SiNW diameter, consisting in forming a thermal silicon oxide shell around a pure SiNW at the desired thickness, and simply removing it with an fluorhydric acid solution. Alternatively, a plane-dependant wet etching can be performed alone in order to realize 1D nanostructures [10], [11]. Another method involving pre-fabricated structures (like nanowires, nanoparticles) as a hard mask can avoid the costly use of EBL to define the patterns [12], but this requires additional steps of the pre-fabricated structures transfer and alignment. The nanoimprint technique has also demonstrated the

possibility to fabricate metallic NWs as thin as 10 nm, involving a superlattice selectively etched as a stamp [13].

These last examples report the fabrication of nanowires parallel to the substrate (horizontal NWs). Nevertheless, with the intention of saving place on the substrate, efforts have been done to fabricate vertical nanowires. This leads to a higher nanostructure density, essential for a massive device integration. The principles are basically the same as the ones mentioned above. Hausmann et al. used Au nanoparticles as a hard mask for inductively-coupled plasma (ICP) RIE of diamond NWs [14], Hsu et al. used silica nanoparticles to fabricate SiNWs down to 60 nm in diameter with simple RIE, directly etched from the Si substrate [15]. Geyer et al. used a porous alumina template to define small pits into the surface of the substrate thanks to RIE [16]. The originality of the latter method is the metal-assisted etching of the substrate, which is used instead of classical plasma-based etching. Each pit receive a particle of a noble metal (here Ag) that will catalyze the downward wet etching of the Si substrate, leading to SiNWs < 20 nm in diameter.

However, all these methods always rely on the definition of small patterns, often on the subsequent etching of nanostructures through the mask thus defined. They may allow the fabrication of complex structures ([16]), but they are usually considered as being heavy, time-consuming and not easy to use.

Bottom-up techniques

The bottom-up method consists in assembling atoms or molecules to form bigger structures, generally using self-assembly rather than heavy methods based on single atom displacements, which don't lead to large areas of nanostructures. Self-assembly is defined as a spontaneous event occurring between neighbouring atoms or molecules, leading to the creation of bonds between them, which will form bigger structures as long as these events occur. They are usually of a chemical nature: redox reactions or molecules cracking leading to the incorporation of additional atoms on the already-existing formation. Of course a continuous supply of the source material is needed to achieve the growth, and several techniques are reported, depending on the conditions the nanostructures are formed.

An emblematic method, that led to the first formation of the well-known carbon nanotubes [17], is the arc discharge. Originally consisting in applying a potential between two graphitic electrodes (to provide carbon), the composition of the electrodes can be changed to form another type of nanostructure. First, the graphite electrodes were enriched with metallic catalyst to get SWCNTs (only MWCNTs are obtained with pure graphite electrodes). Then, Si crystals incorporated inside the graphite electrodes led to SiNWs [18]. The same team managed to obtain ZnO NWs by inserting a ZnO/C powder mixture in the cathode [19], and another team obtained a wide variety of ZnO nanostructures (from pure Zn electrodes), which shows the high selectivity of the process, in that particular case [20].

The source matter can be supplied in the liquid form, like in solution-based techniques. The latter often have recourse to a supercritical fluid, which is a fluid heated

above its critical temperature and compressed above its critical pressure. Such a fluid has a high dispersion potential, and both metallic catalyst and precursor enrich this fluid. SiNWs have been synthesized this way using Au nanoparticles, diphenylsilane ($SiH_2(C_6H_5)_2$) as a precursor and hexane as liquid media [21]. Heated above the precursor dissociation temperature (and therefore above the Au/Si eutectic temperature), Si atoms and Au form an alloy that, when saturated with Si, will lead to SiNW formation (see Growth theory section below). This method has led to highly-crystalline SiNWs with diameter as low as 4 nm. Other catalysts have also been used with success: Ni [22], Cu [23]. Another group managed to synthesized highly-crystalline III-V compounds NWs with a similar technique: using low melting point metals as catalyst and organometallic precursors, fibres with diameters as low as 10 nm have been produced, at relatively low temperatures [24].

The electrodeposition method also utilizes the liquid media to grow nanostructures. Here again a precursor is used as the carrier of the material to grow, but an electric field is applied to enhance the chemical reaction. This topic has already been treated in chapter 2, where references about 1D nanostructures growth via inside porous templates are provided.

As for molecular beam epitaxy (MBE), the source material is supplied via a gas-phase. Ultra-pure solid material(s) is (are) evaporated onto a substrate, and an epitaxial quality can be obtained. Since ultra-pure materials are used, a ultra-high vacuum is required to prevent any oxidative species from contaminating the chamber. The pressure is thus decrease down to 10^{-10} Torr. Depending on the kind of material one wants to grow, a catalyst may be required. In the case of SiNWs, Au is often deposited as a thin film that breaks up into nanoparticles when heated [25]. A great advantage of MBE is that complex heterostructures are easily achievable, thanks to an accurate control of the species flows. Thus, a wide variety of other compounds, especially type III nitrides (binary or ternary like GaN [26], AlN [27], InN [28], InGaN [29]...) and III-V (GaAs [30]) compounds have been synthesized as nanowires, sometimes with the help of a plasma (Plasma-assisted MBE). The nanowires thus obtained are generally of a high crystallinity. It is found that a growth may occur even without catalyst, like GaAs NWs [31], InAs [32], thanks to the deposition of SiO_2 thin film, which precise role hasn't been defined yet. One of the main drawback of MBE is the impossibility so far to grow Si nanowires with diameter below 40 nm.

The chemical vapor deposition (CVD) process is also based on a gaseous compound. Contrary to MBE, one don't use pure evaporated material to grow the nanostructures. Instead, a precursor that contains the desired element is injected inside a hot furnace and decomposed onto a substrate, where the atoms of this element gather and form a nanowire or a nanotube thanks to a catalyst. In some cases, for example for SiNW growth, the residues of the precursor decomposition can play a role in the growth. Thus, the silicon tetrachloride ($SiCl_4$) decomposition leads to HCl formation when injected with H_2 inside the furnace, which etches away any undesired silicon oxide. In the case of NW growth, the growth often occurs according to the VLS or VSS mechanism (see the next section). In their review, Schmidt et al. distiguish between low temperature CVD and

high temperature CVD [1]. The relevance of such a separation relies on the choice of the catalyst and of the precursors, which behaviour changes depending on the temperature range. High temperature CVD (T $>$ 700°C) is said to allow the use of a wider variety of catalyst, since a greater energy can make the formation of an droplet alloy easier. A counterpart of using such high temperatures is the so-called Ostwald ripening, known to cause the agglomeration of the small catalyst droplets. This results in a bad control of the NW diameter, and in a minimum diameter rather high. On the other hand, in the case of low temperature CVD, the precursor has to decompose easily with the only temperature. This is why silane is often chosen for SiNW growth, since SiH_4 molecules break around 350°C. In an alternative version of the CVD process, the source material is directly provided by the substrate itself, that reacts with a reactive gas injected inside the reactor to finally form the nanostructure. The well-known plasma-enhanced CVD (PECVD) allows to use relatively low temperature (200-300°C), the energy needed for the growth system being supplied by the plasma. Besides SiNWs, which growth have been widely studied, GaN NWs [33], ZnO NWs [34], [35], but also CNTs [36], [37], [38] have been synthesized using CVD. A CVD spin-off, named hot wire CVD (HWCVD), relies on the same principle, except that a cracking device, i.e a metallic filament resistively heated by a DC current, is inserted inside a CVD reactor. Generally speaking, its goal is to provide energy to the system via another way than temperature or pressure. This can for example helps breaking gas precursor molecules before they arrive on the sample, either if breaking these molecules thermally is too hard, or if the process temperature is limited for some physical reasons related to the sample. This growth method has been used in this work for both SiNW and CNT growths and will be discussed more deeply later in this chapter. The HWCVD allows to reach high deposition rates for thin films [39], [40], to grow SiNWs at relatively low temperature [41], and even to achieve epitaxial deposition under non-favorable conditions [42]. Concerning the work of our team about this method, the reader can refer to [43], [44] and [45].

The laser ablation technique uses a solid target, heated at a high temperature and etched in vacuum by a high-power pulsed laser in order to release nanoparticles containing a catalyst, or both catalyst and precursor in a precise ratio. By colliding with the inert carrier gas, the nanoparticles condense into small clusters and the growth partially starts, with the same principle as in the CVD method described above (alloy, supersaturation and crystallization). Thanks to the gas flow, the nanostructures are collected at the cold end of the furnace. The first use of this technique led to the formation of CNTs, by using a target made of graphite, enriched with Ni and Co [46], [47]. Si and Ge NWs with very small diameter (6 nm and 3 nm, respectively) have been synthesized this way, with the particularity that Fe was used as a catalyst, thanks to the high temperature (1200°C for SiNWs and 860°C for GeNWs) of the furnace [48]. Shortly after, similar results have been published about SiNWs [49], as well as interesting results about boron nitride nanotubes formation, using a Ni and Co mixed with BN in the target [50]. The main advantage of this technique is obviously its versatility, since only the change of the target allows to get nanostructures of a different material. Thus, doped SiNWs can be obtained this way [51].

To control completely the characteristics of the as-grown nanostructures, it is essential to study and to understand the mechanisms that rule their growth. The next section will explain in detail the main principles of the 1D nanostructure growth theory, studied by many research teams since the 1960s.

3.2.2 Growth theory - Influence of the growth parameters

The fundamentals mechanisms involved in 1D nanostructure growth, once modelized, allow a better understanding of the behaviour (shape, growth rate, transport kinetics, crystallinity...) of the nanostructures and therefore a possible control over their properties. Here we will stick on the description of the mechanisms involved in CVD growth, for this growth is the one we chose to grow SiNWs and CNTs (see the Results section), that are the most emblematic 1D nanostructures studied so far. After a general explanation of the basis principles, we will see in what extent the experimental parameters can influence the properties of these nanostructures .

The growth theory in chemical vapour deposition

Depending on the experimental conditions, that is pressure, temperature, species, flow rates..., different mechanisms can rule the growth. Here we will review some of the main ones. Among them, we will dwell more particularly on the Vapor-Liquid-Solid (VLS) mechanism.

The Vapor-Liquid-Solid (VLS) mechanism

Today most of the nanowires are synthesized by using the VLS mechanism, that explains their growth with a succession of simple phase events. The first authors who talked about VLS growth were R.S. Wagner and W.C. Ellis in 1964 [52]. Their paper is based on the growth of Si nanowhiskers, grown thanks to Au impurities, but they extend their theory to a wide variety of systems, even to macroscopic needle that could follow this mechanism. They describe the main steps and requirements for such a growth, rejecting a former theory that required the presence of a screw dislocation. Basically, the whiskers they observed are believed to grow from a precursor in vapor phase that would turn into a crystalline solid phase via an intermediate liquid phase. The coexistence of the three states of matter thus gives the name to the mechanism. They declare the essential presence of the liquid phase, called impurity, or catalyst, for the formation of whiskers. A series of steps is proposed to explain how the gaseous phase leads to a solid nanowire, included what is thought to happen inside the catalyst droplet. These interpretations are still quoted today to explain numerous nanowire growths and are detailed in the following.

For the sake of simplicity, we will consider the SiNW growth. After the transport of the gaseous species (generally SiH_4, Si_2H_6, or $SiCl_4$) to the surroundings of the liquid impurity, that some people consider to be a preliminary step, the gas molecules are adsorbed onto the surface of the liquid droplet (step 1 in Figure 3.1(b)). Then the

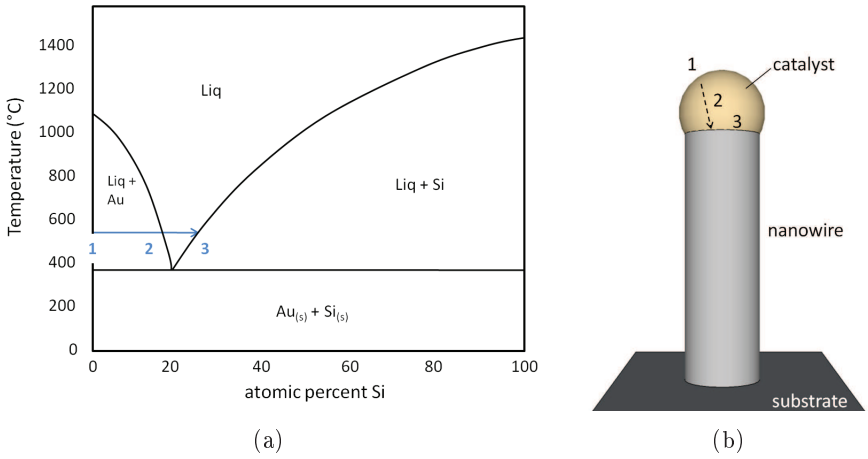

(a) (b)

Figure 3.1: (a) Au-Si phase diagram. (b) Schematic drawing of a nanowire growing in the VLS mode.

catalytic effect of the liquid droplet enhances the dissociation of the precursor, that releases the Si atoms that will constitute the wire. This first step is usually called the incorporation (step 1 in Figure 3.1(a)). Note that the process temperature is often enough to crack the precursor molecules, especially silane, which decomposes at $\approx 350°C$. Due to a concentration gradient inside the droplet, incorporated Si atoms diffuse through it, which is believed to be fast, given the nanometric size of the latter [53] (step 2 in Figure 3.1(b)). As long as the precursor supply is ensured, the Si concentration increases inside the droplet (step 2 in Figure 3.1(a)), until a liquid alloy is formed (zone Liq in Figure 3.1(a)), provided the temperature allows it. The catalyst and the incorporated element have therefore to be chosen so that they can form a low-temperature eutectic phase. In the case of Au-catalyzed SiNW growth, this condition is fulfilled provided the growth temperature is above 363°C. The droplet is rapidly saturated with Si, once Si concentration reaches the liquidus line (step 3 in Figure 3.1(a)). At this moment, Si starts to precipitate at the liquid droplet/solid substrate interface, leading to a crystalline phase that will form the nanowire (step 3 in Figure 3.1(b)). In the steady-state regime, the crystallization continues, pushing the catalyst droplet away from the substrate with the nanowire in between, which growth can continue as long as the liquid catalyst is present, thus leading to very long wires (up to several hundreds of microns). If for some reason the liquid droplet doesn't stay at the tip of the wire, the catalytic growth immediately stops. We will have a more detailed discussion about growth rate and NW diameter, but as a first approximation, we can say that the longer the growth is performed, the longer the final wire. As for the NW diameter, it is strongly related to the size of the droplet/NW interface, and therefore to the diameter of the catalyst droplet at a given instant.

A VLS-like mechanism is also proposed to explain the formation of CNTs under certain conditions of the CVD process. Despite a different final shape compared to

NWs grown by VLS (a tube instead of a plain wire), we find the decomposition of a carbonaceous precursor (CH_4, C_2H_2, C_6H_6, CO...) at the surface of a metallic catalyst, the diffusion of carbon atoms through – or on the surface of – the catalyst until its saturation and finally the formation of a solid nanotube from the catalyst, that is all the same steps cited above, though originally stated for nanowire growth [54]. The reasons why carbon atoms arrange forming a hollow cylinder have been explained in terms of energetically favourable states of the graphitic planes surrounding the metal particle. It costs few energy to form a carbon hemisphere around the particle, and this hemisphere is the start point of the further tubular growth creating the nanotube [55]. Depending on the intensity of the interaction between the catalytic particle and the substrate, two different configurations can be found. Like most of the NW growths, the catalyst can end up at the tip of the CNT; this happens generally in the case of a low interaction between the catalyst and the substrate, and is named "tip-growth" [56], [57]. On the other hand, if the material used as a substrate and the catalyst have more affinities, their high interaction will make the catalyst stick onto the substrate, which will lead to a "base growth" [58], [59]. A base growth has also been reported for SiO_x [60], ZnO [61], boron [62], copper oxide [63]... It has been showed that the size of the catalyst can also influence the growth mode [64]. In this study, particles coming from thin Ni films lead to base growth and particles coming from thicker Ni films lead to tip growth. A mixed mode is obtained for intermediate Ni film thicknesses. For a more detailed review about the various CNT growths modes, the interested reader can refer to the review by Kumar [65].

A very peculiar specificity of the VLS growth is that, if a small particle can catalyse the growth of a narrow nanowire, a lower limit still exists for the size of this catalyst. Indeed, it has been proved that below a critical diameter, no growth occurs no matter the conditions. This has been explained by the Gibbs-Thomson effect, that says that the chemical potential of a particle increases when its diameter decreases. In other words, the smaller a particle, the more energy is needed to add atoms in it. For very small particles, the chemical potential is therefore very high. In the case of VLS mechanism, it can thus be higher than the one of the vapor phase that supplies the precursor, which prevents molecules from being adsorbed on the catalyst surface. The relation between the chemical potential μ of the particle and the particle radius r can be given as:

$$\mu = \mu_{bulk} + 2\Omega\frac{\sigma}{r}$$

where μ_{bulk} is the chemical potential of a particle with an infinite radius (i.e the bulk form of the same material), Ω is the volume of one atom of the particle and σ the surface free energy of the particle. Therefore the chemical potential of a nanoparticle is always higher than the one of the corresponding bulk material. If the particle diameter is exactly equal to the critical diameter r_c, then μ equals the chemical potential of the vapor phase μ_v (by definition of the critical radius) and the precursor molecules start to deposit and decompose on its surface. The particle radius is in this case equal to

$$r_c = \frac{2\Omega\sigma}{\mu_v - \mu_{bulk}}$$

The Vapor-Solid-Solid (VSS) mechanism

If the temperature is not high enough, the liquid phase cannot form. This is the case when the process is temperature-constrained, i.e it can't bear a too high temperature, or more simply if a couple of elements has a very high eutectic temperature (for example T_{eut}(Fe/Si)$\approx$ 1200°C). In such a case, the VLS mechanism can't be applied anymore to explain the nanowire growth. Since the growth occurs at a low temperature (i.e under the eutectic temperature), all the system (catalyst, wire) should remain in a solid phase, hence the VSS appellation. However, the mechanism is quite similar to the VLS one. Still taking the Au/Si as an example (the phase diagram is very simple), we see that the decomposed Si-based molecules (SiH_4, $SiCl_4$, Si_2H_6...) deposit on Au and form a solid Au/Si alloy after the Si incorporation. In the same way as the VLS mechanism, Si will diffuse in the solid alloy and finally crystallize when the alloy is saturated with Si. According to the Au-Si phase diagram, the $(AuSi)_{(s)}$ solution exists until a very high Si concentration (almost 100 %), therefore the saturation of the droplet alloy is expected to be longer than for the VLS mechanism. Another direct difference inherent to the VSS mechanism is that the growth rate is expected to be lower as well, for two main reasons: first, the adsorption probability of Si atoms is decreased because of a higher chemical potential of the catalytic droplet, and secondly the diffusion rate of Si through the solid Au droplet must be lower than in liquid Au.

A basic hint for determining which type of growth is occurring (though not quantitative) is to observe the shape of the catalyst during the growth. If the droplet is liquid, it exhibits a curved, ball-like surface, whereas a solid catalyst will present a faceted surface with sharp edges, forming a solid polyhedron at the tip of the nanostructure. Nevertheless, it has been shown that the only process temperature couldn't determine whether the catalyst droplet is liquid or solid, some size effects having an influence on the phase diagram itself. Kodambaka et al. ([66]) showed for example that the thermal history, as well as the supersaturation of Ge in the droplet could lead either to a liquid alloy below the eutectic temperature, or to a solid alloy above the eutectic temperature, revealing a hysteresis behaviour in the phase transformation, intensified at the nanometric scale.

The Solid-Liquid-Solid (SLS) mechanism

The major difference of this growth mechanism, compared to the two previously mentioned is the nature of the source material. If the global system works in an analogous way, in this case the material source is in solid phase, not gaseous like in VLS or VSS. The particularity is that the substrate itself acts as a supplier regarding the metal catalyst, deposited on its surface before the growth. For this reason, and since silicon is the most widely used material for substrates, a lot of studies reporting such a growth deals with SiNW formation. Wong et al. reported a Au-catalysed growth under a nitrogen flow [67] that gave quasi-aligned SiNWs, growing off the substrate. Earlier, Yan et al.

used Ni particles as catalyst, and synthesized amorphous SiNWs [68], [69]. The latter examples used high temperatures to approach the catalyst-Si eutectic temperature. Because the In-Si has a low melting point at any concentration, Yu et al. managed to grow crystalline SiNWs with relatively low temperature ($< 500°C$) [70]. In the latter case the growth is in-plane because the Si supplier was a Si thin layer (deposited on an ITO substrate), which force the growth the NWs to stay in-plane. Composite nanowires like gold-silica [71] and silicon carbide [72] have also been synthesized using a solid source for SLS growth.

Controlling the nanostructures properties

Controlling and understanding the mechanisms explained above can allow to tailor the nanostructure properties, that are geometrical aspect (length, diameter, number of walls for nanotubes, general shape...), cristallinity (relative amount of the crystallized phase, crystalline orientation), orientation of the nanostructure... All these properties will impact the nanostructure behaviour, when inserted in functional devices, and are therefore of capital interest. In the following we will review some of the many studies which investigated the growth parameters that influence these properties. We naturally focus on SiNWs, since we studied their growth during this thesis.

An early work has been published in 1997 about SiNW growth, catalyzed with gold [73]. The nanowire diameters and their defects have been studied more particularly. It was found that a higher silane partial pressure (1 Torr) led to more defects in the wires, and especially to sudden growth direction switching, forming "kinks" in the nanowires rather than growing straight. It was then proposed that a higher silane partial pressure led to a higher growth rate, since more Si atoms are adsorbed on the droplet alloy surface. Therefore more instabilities should occur at the liquid/solid interface, which creates defects during the growth. A low silane partial pressure (0.01 Torr) gave straight, defect-free SiNWs, attributed to a low growth rate. A higher temperature (here 520°C) also acts in favour of a low amount of defect, due to a higher mobility of the species, notably at the liquid/solid interface, which improves their crystalline arrangement. This would also normally make the nanowires straighter than if grown at a lower temperature (generally speaking) [73], [74]. Nevertheless, it has been shown that a too high temperature was not good if thin nanowires were desired, since agglomeration of catalyst droplets is favoured [75], [76]. Increasing the silane partial pressure can, on the contrary, enhance the growth of thin SiNWs. Indeed, the chemical potential of vapour is then increased, which decreases the value of the critical diameter of the droplet which has been presented a few paragraphs above (p.69).

We have seen that pressure and temperature are important parameters to pay attention to since they highly impact kinking, diameter, growth rate... Another important parameter is the nanowire diameter itself, that is, as strongly related to it, the size of the catalyst particle and its shape in a general way. Numerous articles report a diameter dependence of growth rate, but also growth direction and crystalline planes orientation. Thus, it has been shown that when grown from Au particles, SiNWs preferentially turn towards the $<110>$ direction when smaller than 20 nm in diameter [77]. For larger

diameter (> 30 nm), the <111> direction is preferred whereas intermediate diameter predominantly gave <112>-oriented NWs. Furthermore, it had been previously shown that the crystalline orientation of the substrate had nothing to see with the NW orientation, since the same phenomenon has been observed for SiNWs grown on an amorphous SiO_2 layer [78].

A lot of articles can be found about the diameter dependence of the SiNW growth rate, and can appear contradictory. Several decades ago, Givargizov noticed that thicker NWs grew faster than thinner ones [79], as well as Kikkawa et al. [74]. In both cases the rate-limiting step was assumed to be the decomposition/incorporation of Si atoms in the catalyst droplet (step 1 in Figure 3.1(b)). Nevertheless, these observations have not always been confirmed. Dhalluin et al. did find such a diameter-dependence, but only for SiNWs with diameter smaller than 100 nm, observing the reverse for thicker NWs [80]. As well as Schubert et al., who observed a decreasing growth rate with an increasing NW diameter [25], and Weyer quite earlier [81]. In 2006, Kodambaka even found a non-dependence of the growth rate on the NW diameter [82]. An essential article from Gosele's group brings all these apparently contradictory observations together: claiming that there must be more than a single rate-limiting step, they developed a model that takes into account the interplay of both incorporation and crystallization, and found that opposite diameter dependencies can be found depending on the growth conditions [83]. After defining analytical expressions of the incorporation and the crystallization velocities, they end up with the following general expression for the steady state velocity:

$$v = v_0 + \Gamma \frac{2\Omega\sigma}{r}$$

where Ω, σ and r represent the molar volume of Si, the surface tension of Si, and the radius of the NW, respectively. Γ is the most important parameter of this formula, since its sign gives directly the variation sense of the growth rate with respect to the NW diameter. Γ is expressed as a function of both the derivatives of the incorporation rate (noted α) and the crystallization rate (noted ω) with respect to the supersaturation (that is the chemical potential difference between the vapour and the solid NW). This magnitude is negative if either one or the other rate is rate-limiting. Therefore the growth rate is expected to increase with an increasing diameter. But in the very specific case where $\alpha < \omega$, Γ appears to become positive, thus giving an opposite growth rate dependence on the NW diameter. This way they are even in accordance with Kodamabaka [82], in the case where the incorporation rate is supersaturation-independent. This gives $\alpha \to 0$, $\Gamma \to 0$, and thus a constant growth velocity. Before determining whether the diameter has an influence on the growth rate or not, some factors can definitely impact the diameter of the nanowires. As already mentioned, the Ostwald ripening makes the droplet catalysts merge and form bigger droplets for increasing temperature, which invariably leads to thicker nanowires. Another factor that impacts the nanowire diameter is the catalyst migration during the nanowire growth. For example, if some gold atoms migrate from the Au droplet to the growing SiNW sidewalls, this will result in a smaller catalyst to continue the growth, and therefore to a smaller nanowire. If this mechanism happens continuously, the nanowire exhibits a conical shape, with a diameter decreasing from

its base to the tip. This phenomenon is called "tapering" and has been studied in [76]. The authors assume that this can happen in ultra-high vacuum conditions, where contaminants in the catalyst droplet don't prevent Au from migrating.

Finally, some examples of investigations can be given for other types of nanowires. The growth rate of InN NWs as a function of temperature, In pressure, and deposition time has been studied in [28], and the general aspect of ZnO NWs depending on growth temperature in [84]. GaN NWs have been synthesized by plasma-assisted MBE in [29], and it has been shown that an increasing temperature (800°) led to thinner nanowires, with a lower density.

A CNT can be composed of a single graphene sheet, and therefore called "single-wall" CNT (SWNT), or of several concentric graphene sheets, which forms a multi-wall CNT (MWNT). If CNTs are considered for electronic devices, it is of capital interest to control the number of walls during their synthesis. Indeed, the chirality of a CNT, which dictates its electrical behaviour (i.e. semi-conducting or metallic), can't be controlled. Therefore, statistically, a MWNT will contain a metallic tube and the whole MWNT will thus be metallic. The only way to get semi-conducting CNT is therefore to synthesize SWNTs, which exhibit a semi-conducting behaviour in two cases out of three [85]. Kumar and Ando [65] showed that CNTs can be selectively grown with CVD. A high growth temperature ($> 850°C$), as well as a low catalyst concentration lead to a higher SWNT/MWNT ratio, and a low gas pressure favours the synthesis of SWNTs. The nature of the catalyst is also of utmost interest to catalyse SWNTs by CVD, as explained by Kitiyanan et al. [86] who used a Co-Mo alloy as a catalyst and CO as gaseous precursor. Laser ablation also led to a high selectivity in SWNT synthesis [87], as well as arc discharge technique [88].

3.2.3 Guided growth - Confined growth in porous templates

If some structures naturally grow in one dimension only, some others wouldn't without the help of a guide. Several methods allow to force or to favour the growth along a particular direction, like on edges of pre-structured surface, on certain crystallographic planes, and inside porous templates. Unlike the "free growth" methods, these methods allow to control the orientation of the nanostructures, which is of capital interest for a subsequent potential use in an electronic device.

A well-known method involves the relief patterns of a solid surface, that can direct the growth of 1D nanostructures. Either the elements preferentially nucleate along some edges pre-formed before the growth [89], [90], or the shapes defined on the substrate prevent any formation anywhere other than planned (shadow sputtering) [91]. Metallic and semi-conducting NWs have been synthesized this way, the template patterns being realized by lithography, but also via an interesting technique that uses the cross-section edges of a multilayer [92]. These techniques can lead to the formation of nanowires as thin as 15 nm (shadow sputtering) and are grouped together in Figure 3.2, which is an extract from [5].

Another way to organize the growth of 1D nanostructures is to use already-existing nanostructrues as a support for a subsequent growth. Of course a first nanostructure

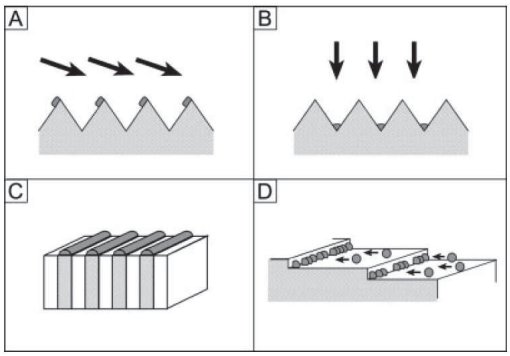

Figure 3.2: This figure is extracted from [5]. (A) refers to shadow sputtering [91], (B) and (D) to preferential nucleation [89], [90] and (C) to multilayer-based template [92].

synthesis is required, but this technique is employed to fabricate structures that couldn't follow a one-dimensional growth by themselves, and thus need a first support to grow. One can thus realize multi-layered, coaxial wires with different materials, thus forming a core/shell structure. The initial supporting nanostructure can be usual, like nanowires [93], CNTs [94], but also biomolecules, like DNA [95]. The selective removal of the inner part can lead to hollow 1D nanostructures.

A more detailed overview of the existing techniques has been done by Xia et al. in 2003 [5] and gives many interesting references that wander off our work a bit. We would like to focus more on reviewing the growths carried out in porous materials. Many porous materials exist and can guide nanostructure growth, but those which exhibit straight and vertical pores are in the big majority of cases porous anodic alumina, and track-etched polymer films. Both are commercially available, nevertheless, PAA can be easily "home-made" and is therefore tailorable. Besides, the PAA pores are usually straighter and have a higher density than porous polymer films [5]. The examples of PAA-templated growth are numerous, and complete those given in the first section of chapter 2: CNTs [96], [97] and [98], [99]..., metallic NWs [100] or NTs [101], and even a mix of several types of structures [102], [103], leading to great potentialities if used as building blocks for inter-connections in electronic nano-devices.

Of course SiNW growth in PAA is also widely reported, especially by Redwing's group [104], [105], [106]. One can quote Lombardi et al. [107], who used PAA only for localized gold evaporation through its pores and then removed it before performing the SiNW growth, David et al. [108], who deposited gold from colloid using electromigration, and Zhang et al. [109], who used AC electrodeposition with $AuCl_3$ solution. All the growths are generally performed by CVD, using SiH_4 or $SiCl_4$.

We have seen that there are plenty of methods to synthesize 1D nanostructures, and that the properties of the latter depend a lot on the growth conditions, which can be understood provided the growth mechanisms are known. The following section is dedicated to the presentation of our experiments, and the results we got from our attempts to synthesize CNTs and SiNWs inside PAA templates.

3.3 Experiments, results and discussion

Given all the information previously detailed, we have grown some 1D nanostructures inside porous alumina templates. As already explained, the most popular and investigated ones are the SiNWs and the CNTs, though a lot of other materials are still being studied nowadays. The challenge of this section is to bring a proof of feasibility of a confined growth inside alumina pores (though already reported in the literature), but also to manage to connect the as-grown nanostructures, and observe a current flowing through them, from one tip to another, that is from the top of the sample to the silicon substrate.

3.3.1 The hot wire CVD reactor

This paragraph describes the experimental equipments that we used for all the nanostructure growth (both CNTs and SiNWs). For every nanostructure growth, we used the CVD process, already described in p.64, in tubular quartz furnaces. In order to avoid to mix many different gaseous species, i.e not to contaminate them, each of them was exclusively dedicated to one type of growth, with its own gas lines and pumps. Both furnaces are quite classical, but have the particularity to be equipped with a tailor-made hot wire (HW) system, thus creating a HWCVD reactor. The HW part is of high interest for processes that require a supplement of energy, that cannot be provided with the only temperature (see p.64).

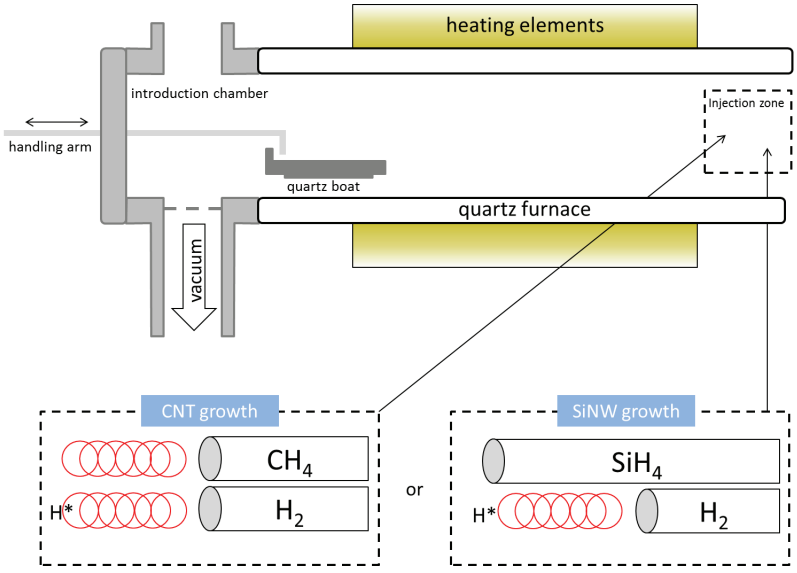

Figure 3.3: Schematic drawing of the Hot-Wire CVD reactor used for the 1D nanostructure growth.

A schematic drawing of our HWCVD equipment is shown in Figure 3.3. In the case of SiNW growth, only one inlet is equipped with a hot wire (often called filament), since

silane doesn't need any extra energy to decompose in the temperature range that we usually use ($> 450°C$). On the other hand, for CNT growth, both H_2 and CH_4 inlets open onto two dedicated filaments, that crack H_2 molecules on one hand, and CH_4 on the other. The filaments are hand-made from a high-purity (99.95 %) tungsten wire, and twisted so as to form 10 turns, in a spring shape. It is inserted into two molybdenum holders, themselves connected to a power supply via metallic rods passing through the quartz tube closing cap. By applying a voltage of a few volts (typically 10-15 V) between both ends of the HW, it can be heated up to $\approx 2000°C$. Gas flows are computer-controlled and can be set from 0 to 100 sccm. A thermocouple going along the gas inlets measures the temperature, automatically adjusted to the set-point. The heating of the reactor is ensured by surrounding resistive elements, located outside the tube. On the other side of the furnace is located the introduction chamber, where a steel arm allows the handle of a graphite boat, support of the samples. A turbo-pump is connected to the furnace near the introduction chamber, and flows into a primary pump. This pumping system can typically pump the reactor down to 10^{-6} mbar. The opening of the reactor for the loading of the sample is ensured thanks to a nitrogen inlet, located near the introduction chamber, that puts the reactor at the atmospheric pressure.

3.3.2 Influence of some growth parameters

As said in the first section of this chapter, the goal of this part is to study the growth of 1D nanostructures inside PAA templates. CNT growth inside vertical PAA has already been performed by our team [110], but no SWCNT, and therefore no semiconducting CNT has been grown. We therefore focused more particularly on the SiNW growth, the latter being theoretically naturally semiconducting.

The research of optimized growth conditions

As a basis to start our experiment, we anodized Al layers deposited on Si substrates as described in chapter 1. Sulfuric acid was used for the anodization, and Cu was electrodeposited as a catalyst, as described in chapter 2. A typical view of such a sample before growth is visible in Figure 3.4, where particles with an average height of 200 nm dwell at the bottom of cylindrical pores 30 +/- 5 nm in diameter. This would correspond to an equivalent volume of Cu spheres ≈ 64 nm in diameter. Looking at the Cu-Si phase diagram, it is clear that the temperature range we use for our experiments ($< 600°C$) won't allow the formation of a liquid alloy, the Cu-Si eutectic temperature being above 800°C (Figure 3.5). Except if some nanoscale-related effects occur, we therefore expect the SiNWs to grow under the VSS mechanism.

As already mentioned in a previous article [45], a big challenge of in-pore growth is to prevent the formation of parasitic amorphous material on the sample, which could lead to the clogging of the pores, and thus to the end of the growth. This is the main role of H_2, injected and cracked by the hot wire into atomic hydrogen, that will act as an etching agent regarding amorphous silicon (a-Si). The following describes the route we followed until the first observation of a SiNW growth. For this preliminary study, several

parameters have been varied, namely the global pressure (2.5 to 7.5 mbar), the H_2:SiH_4 ratio (100:20 to 97.5:2.5 sccm), the reactor temperature (490°C to 540°C), as well as the filament temperature (we will speak in terms of filament power in the following: 0 W to 215 W, that is up to $\approx$ 2000°C). We therefore tried to find an operating point that could give SiNWs protruding out of the pores, with few amorphous material inside the pores and on the surface of the sample. All the experiments attempted in the following lasted 30 minutes, and every growth was preceded by a 5 min pre-treatment with atomic hydrogen (H_2 = 100 sccm, total pressure = 5 mbar) at the growth temperature in order to "clean" the sample.

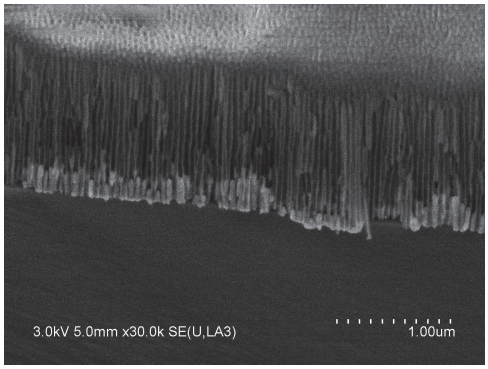

Figure 3.4: SEM cross-section of a PAA with Cu catalyst particle, before SiNW growth.

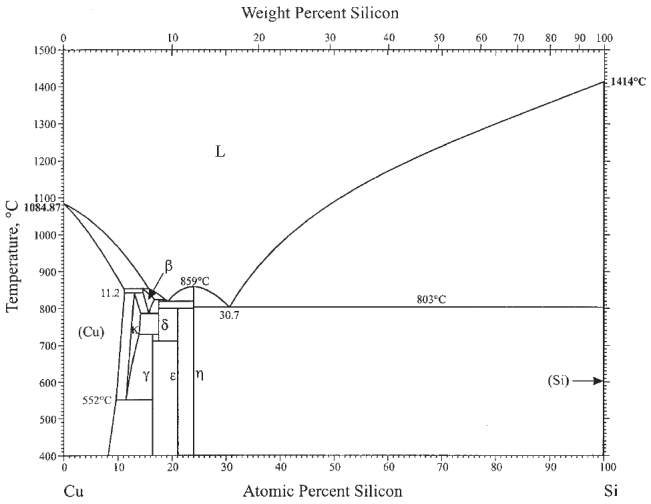

Figure 3.5: Cu-Si phase diagram, from [111].

A first attempt was performed, trying to see any influence of the hot wire power. We used H_2:SiH_4 = 100:20 sccm, p = 7.5 mbar, and T = 540°C. No matter how high the hot wire power was increased (in our equipment limitation), the sample was always found

supporting a huge amount a amorphous material (Figure 3.6). Too much silicon seems to arrive too rapidly over the substrate, with too much energy, which covers immediately all the sample, making the atomic hydrogen useless in that case, since the etching rate couldn't overcome the a-Si deposition rate. A lot of SiNWs are visible, but the undesirable amorphous Si is so cumbersome that we can't conclude anything about their origin. Less extreme conditions have therefore to be found. We therefore set the hot wire power to 175 W, and progressively reduced both the global pressure and the silane flow rate. Indeed it appeared that reducing only the silane flow rate down to 10 sccm (keeping H_2 = 100 sccm) was not enough, since we still found a lot of a-Si onto the sample after the growth. With these reductions, one can finally see some improvements. The influence of silane flow rate is illustrated in Figure 3.7, which gives an example of a sample after a growth performed at p = 4 mbar, with H_2:SiH_4 = 95:5 sccm, and then H_2:SiH_4 = 97.5:2.5 sccm. The surface is clearly cleaner with these "softer" conditions; one can even see the opening of the pores on the top-view in Figure 3.7(b). Nevertheless, and this is visible both in a cross-section view and in a top view, the apparent pore diameter has dramatically decreased because of a non-controlled deposition of a-Si, estimated to 13 +/- 3 nm-thick when SiH_4 = 2.5 sccm, on the sides of the pore walls. The average pore being originally 30 nm in diameter, it is not surprising to find the pores almost completely clogged. This diameter decrease considerably reduces the supply of Si atoms towards the Cu particles, therefore the growth has very few chance to occur in these conditions. After several other attempts, we finally found a very interesting operating point, by keeping the silane flow rate to a very low value (H_2:SiH_4 = 97.5:2.5 sccm) and decreasing the pressure down to 2.5 mbar. In these conditions, the Si atoms supply seems to suit well with respect to the gas penetration inside the pores, and is sufficiently small to preserve the pore walls from parasitic deposition while the NWs are growing. Indeed, the cross-section shown in Figure 3.8 brings some evidence that a growth happened inside the pores in these conditions. First of all, one can clearly see that the Cu particles (appearing in brighter contrast on SEM pictures and highlighted with dotted circles) have migrated during the growth, pushed upwards by the growing SiNWs. Besides, this statement is supported by the presence of a material appearing in light grey, visible underneath every "lifted" Cu particle, that contrasts with the dark black above the Cu particle, and that corresponds to the empty part of the pore (an example is marked with the white brace in Figure 3.8).

Despite these growth evidence, a non-negligible amount of a-Si is present on the pore walls. We therefore decided to investigate the influence of the temperature, expecting that reducing it can limit the formation of a-Si. The same experiment as the one presented in Figure 3.8 was performed at 490°C, but revealed no growth evidence. Indeed, the Cu particles have been found remaining at the bottom of the pores, with no apparent Si precipitation under them. However this temperature decrease has been convincing regarding the limitation of the a-Si formation. The pore walls look smoother and thinner than in the sample at 540°C. We thought that this absence of Si over all the sample is due, on one hand, to an efficient a-Si etching by the atomic hydrogen, but also to a too short deposition time. Indeed, it is well-known that the growth rate is temperature-

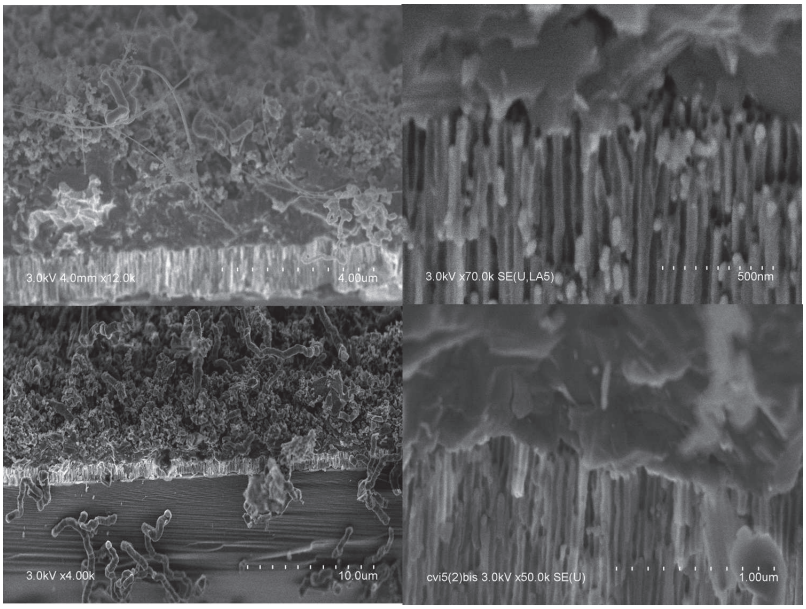

Figure 3.6: SEM cross-sections of a sample after a growth performed at 540°C, P_f=175 W, 7.5 mbar, H_2:SiH_4 = 100:20 sccm.

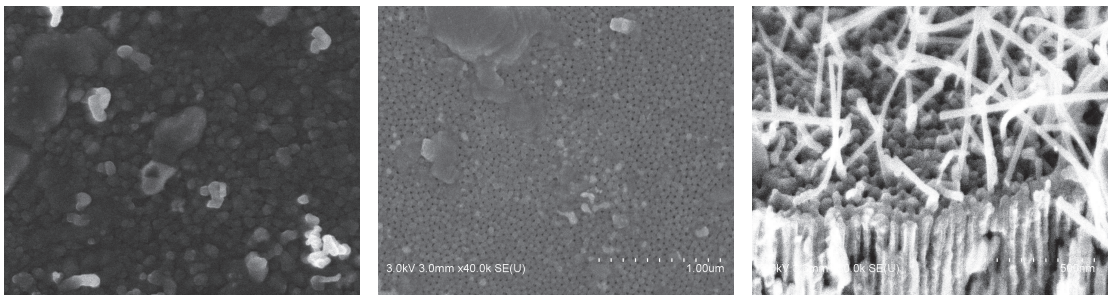

(a) (b) (c)

Figure 3.7: SEM top view of a sample after a growth performed at 540°C, P_f=175 W, 4.0 mbar, (a) H_2:SiH_4 = 95:5 sccm, (b) and (c) H_2:SiH_4 = 97.5:2.5 sccm.

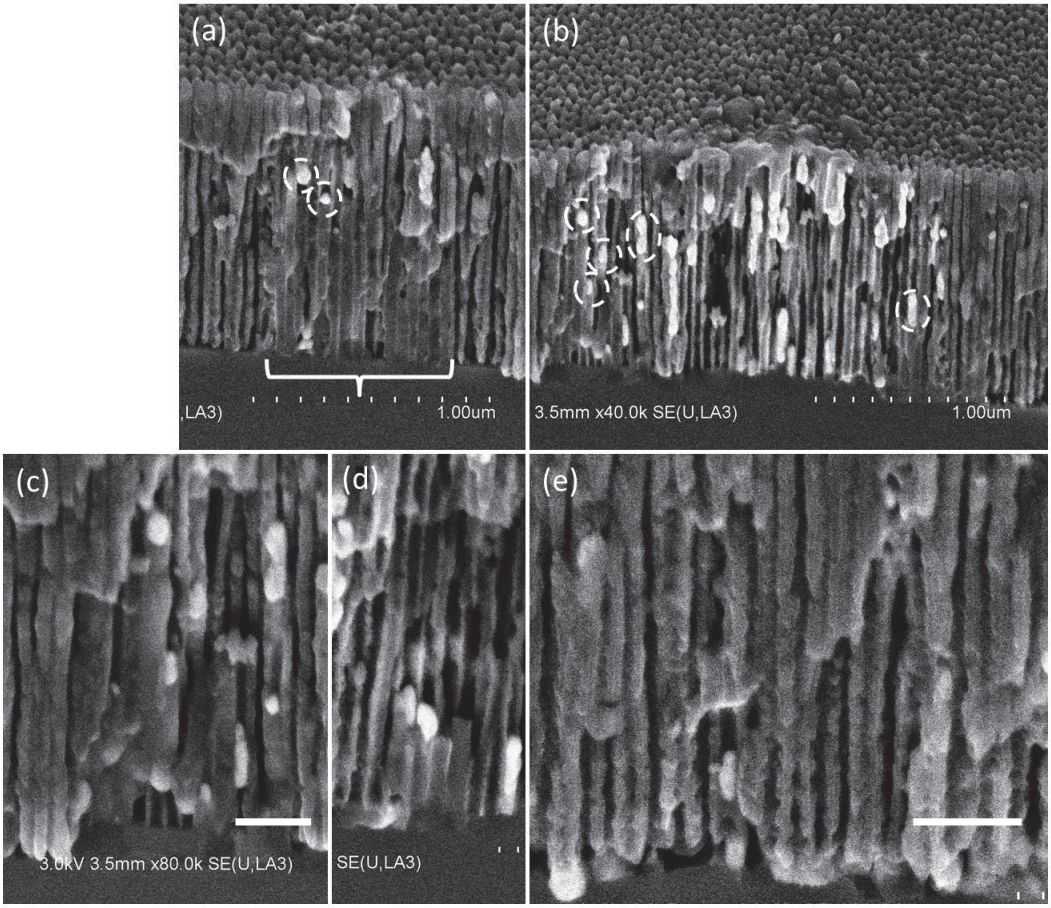

Figure 3.8: SEM cross-sections of a sample after a growth performed at 540°C, 2.5 mbar, P_f=175 W and H_2:SiH_4 = 97.5:2.5 sccm. (a) to (d) some examples of SiNWs with their corresponding Cu particles on their tips, (e) a higher magnification of the enlarged walls due to a-Si deposition. Scale bars in (c), (d) and (e) are 200 nm.

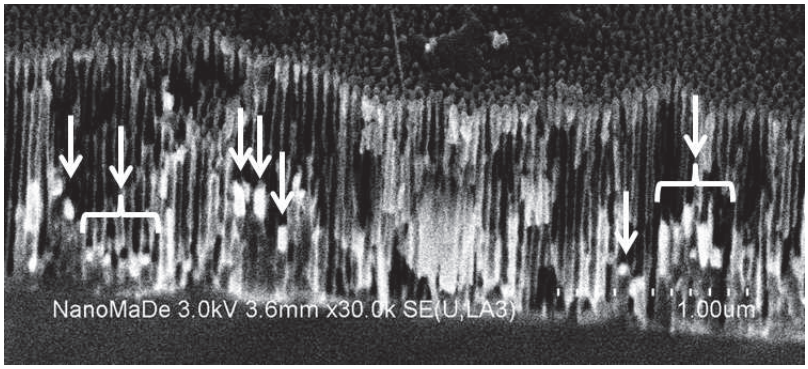

Figure 3.9: SEM cross-section of a sample after a 1 h growth performed at 490°C, 2.5 mbar, P_f=175 W and H_2:SiH_4 = 97.5:2.5 sccm.

dependant (the higher the temperature, the higher the growth rate, see 3.2.2), so we assumed that to reduce the temperature caused the decrease of both the incorporation and the diffusion rates, and therefore delayed the saturation of the Cu-Si alloy. Though 30 minutes were thought to be enough to start a growth, one must remember that the mechanism expected to govern the growth is VSS, which is known to be quite slower than VLS. Furthermore, the confinement of the catalyst inside the pores dramatically reduces the surface exchange with the precursor molecules, which is limited to a circle the diameter of the pore, when a bigger hemispherical surface can react in the case of growth on free surfaces. In order to be sure that a growth could be initiated in these conditions, we performed a longer experiment, expecting that 1 h would be enough for some Cu particles to incorporate Si and reach the saturation. A similar result as the previous experiment was observed inside the pores, that is lifted Cu particles with light grey material, thus proving the possibility to grow SiNWs in these conditions with a longer time. Besides, thanks to the lower temperature, the pore walls were found to be far thinner than at 540°C, since almost no a-Si has deposited on them (Figure 3.9). These optimized conditions are summed up in Table 3.1.

Reactor temperature	Pressure	H_2:SiH_4 ratio	Hot wire power	Growth duration
490°C	2.5 mbar	97.5:2.5 sccm	175 W	60 min

Table 3.1: Optimized growth conditions for SiNW growth in PAA in our HW-CVD reactor.

Some interesting aspects have been revealed by selectively etching the PAA template after the growth, just like it has been done after the electrodeposition step in chapter 2. We found a surprisingly high number of vertical rods remaining after the chemical etching (compared to our expectations based on the filling efficiency of Cu particles in Figure 3.4), and a thin porous layer, estimated at $\approx$ 50 nm-thick, has been found onto the top of these structures (Figure 3.10(b)). Concerning the latter, it is clear that it has been formed during the growth from all the deposited a-Si despite the atomic hydrogen. The shape of this layer is a perfect replica of the underlying PAA, and resists to the PAA

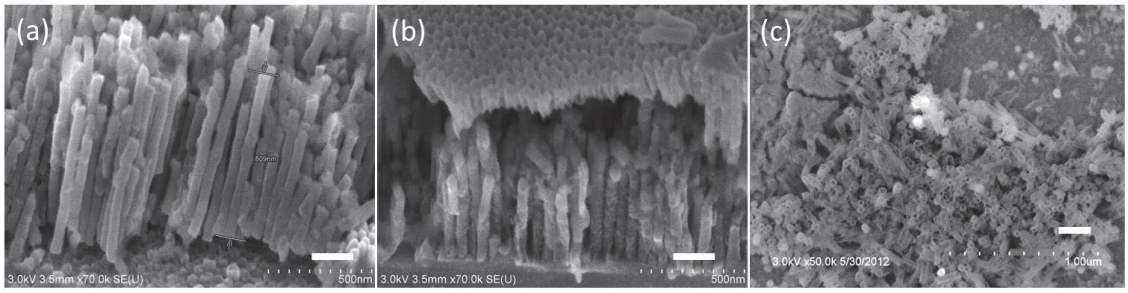

Figure 3.10: Tilted views of the sample shown in Figure 3.9 after PAA wet etching. The hollow structure is clearly visible in (c). Scale bars are 200 nm.

etching, which supports this assessment. Thus, to observe the as-grown nanorods, this crust needs to be removed. This has been done with ICP RIE, using SF_6 and O_2 (35 and 5 sccm, respectively) at 10 mTorr for 7'30 (platen and coil powers were set to 50 and 0 W, respectively). A top view observation thus gives an explanation about this abnormally high number of vertical rods: they actually consist of hollow, tube-like structures, and don't seem to come from a catalytic growth. Indeed, a more probable origin would be that a-Si deposition visible on the pore walls, covering all the inner surface of the pores and thus forming this cylindrical shape, that we call silicon nanotube (SiNT), standing by itself after the PAA removal. Given that every single pore is a potential receiver for a-Si deposition, it is not surprising to find such a high density after the PAA removal. Nevertheless, we will see later (in the TEM investigation part) that we did see some solid SiNWs, which are difficult to discern from SiNTs with the only SEM.

Study of the hot wire power

As mentioned in the previous paragraph, no matter how high the hot wire temperature is, the atomic hydrogen is useless in removing a-Si if the growth conditions are too "extreme", that is if the a-Si formation rate is so high that it forms anyway (high pressure, high silane flow rate...). Note that the term "extreme" has no universal meaning, and has to be taken only regarding our own experimental set up. Given the optimized conditions detailed in Table 3.1, the influence of the hot wire is now clearly discernable when varied once these parameters are set. A simple way to be convinced of the importance of the presence of the hot wire is to perform a growth "wire off", i.e with no current passing through. The results are visible in Figure 3.11 and have to be compared with the sample already showed in Figure 3.9.

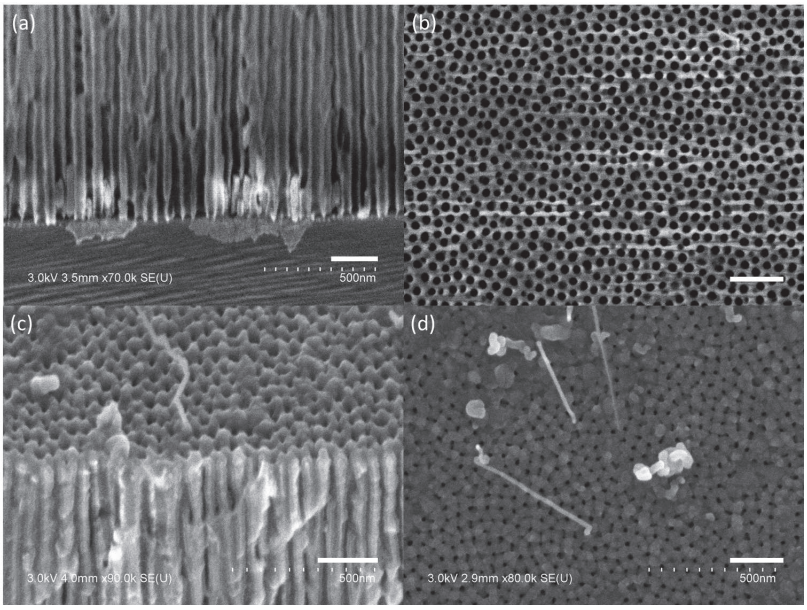

Figure 3.11: (a) and (b): SEM cross-section and top-view of the sample before the growth. (c) and (d): same sample after a growth in optimized conditions (see Table 3.1) with the hot wire off. Scale bars are 200 nm.

The sample clearly exhibits the characteristic features of a-Si-contaminated walls, with this fluffy, dust-like material. The pores got thinner, which is more visible in the top-view picture. This definitely proves the essential presence of atomic hydrogen, and thus of the hot wire for getting rid of a-Si during the growth.

Increasing the hot wire power up to 215 W ($\approx 2000°C$) didn't make any noticeable change on the SiNWs, and we found a similar a-Si crust usually deposited onto the PAA (Figure 3.12). Numerous growth evidence have been found in cross-sections, just like in the sample shown in Figure 3.9, which shows that the growth is not much impacted by the filament power.

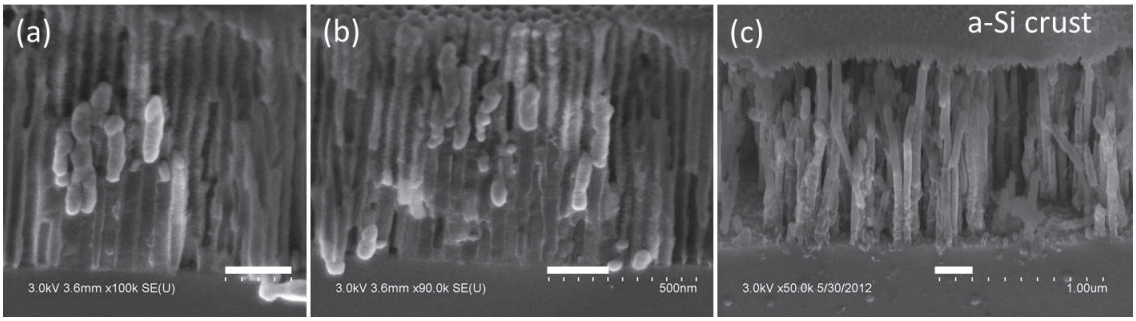

Figure 3.12: (a) and (b) SiNW growth evidence in SEM cross-sections and (c) tilted view of the Si vertical rods supporting a-Si crust. Scale bars are 200 nm.

The influence of the growth temperature

We have seen that a suitable set of growth conditions can be found around the latter parameters, i.e p = 2.5 mbar, H_2:SiH_4 = 97.5:2.5 sccm, and P_f = 175 W. We showed that the temperature could be decisive regarding the growth rate, since 540°C led to visible growth in 30 minutes, whereas a 490°C growth needed more time (1h) to show some growth evidence. We wanted to extend this study by adding two other temperatures, namely 430°C and 580°C. We investigated post-growth samples at 430°C, 490°C, 540°C and 580°C, before and after the PAA removal. 430°C is far below the temperature for which we observe the first growth evidence, therefore it is normal that no growth evidence was visible in this case neither. However we noticed that the pore walls were almost free of a-Si deposit. They look thinner, better defined, and no NT has been found after the PAA removal. A higher H_2:SiH_4 ratio (90:10 sccm) has nevertheless led to some a-Si deposit on the pore walls. As for the 580°C growth, since SiNWs formed at 490°C, there is no reason why they wouldn't form at higher temperature, and this is what has been observed. Nevertheless, at 580°C, we identified more long SiNWs than for lower temperatures, indicating a general higher growth rate, and we also found some big Cu particles catalysing a growth, which may indicate a higher incorporation or crystallization rate that may have accelerated the saturation of the catalyst.

The influence of total pressure

An obvious consequence of an increasing pressure would be a higher a-Si deposition rate, and this has already been shown above. Conversely, a dramatic change occurred when we decreased the total pressure from 2.5 mbar down to 1 mbar. Indeed, we found that no a-Si crust formed onto the top of the PAA, neither on the pores walls i.e no SiNTs were visible after the PAA removal. No additional etching was needed to observe the Si nanorods from the top, and much less hollow structures have been found after the PAA removal. However, it looks like this low pressure condition makes the SiNWs grow much slower. As can be seen in Figure 3.13, a lot of Cu particles have stayed at the bottom of the pores, and only a few have slightly moved upwards by a SiNW growth.

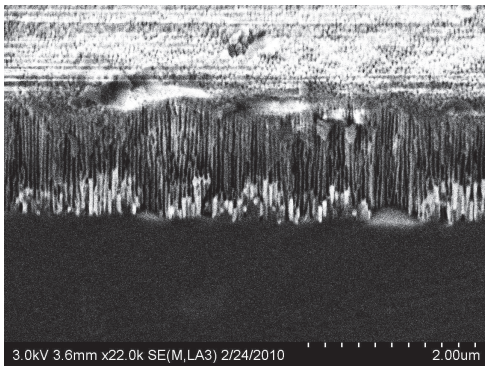

Figure 3.13: SEM cross-section of a PAA after a growth under 1 mbar (540°C, H_2:SiH_4 = 97.5:2.5 sccm, and P_f=175 W.

3.3.3 CNT growth in PAA

As a further study, we wanted to show a certain versatility of our structure, and then tried to grow CNTs in a PAA template. To do so, we electrodeposited Ni at the bottom of the pores as described in chapter 2, and performed a growth in a similar reactor as the one used for SiNW growth. As shown in Figure 3.3, each gas inlet was equipped with its own tungsten filament, in order to crack hydrogen on one hand, and methane on the other. The growth conditions, already optimized for intra-pore growth, were set to a total pressure of 50 mbar, a gas ratio of H_2:CH_4 = 50:50 sccm and a temperature of 500°C, which is known to produce less parasitic carbonaceous species than at higher temperatures. A power of 180 W was applied on each filament, which corresponds to an approximate temperature of 1850°C. Several durations have been tried, until some CNTs protrude out of the template. Figure 3.14 shows four top-views of the sample after a 30 minutes growth with increasing magnification. The picture in the bottom-right corner allows us to make out some CNTs growing out of the PAA, marked with yellow arrows.

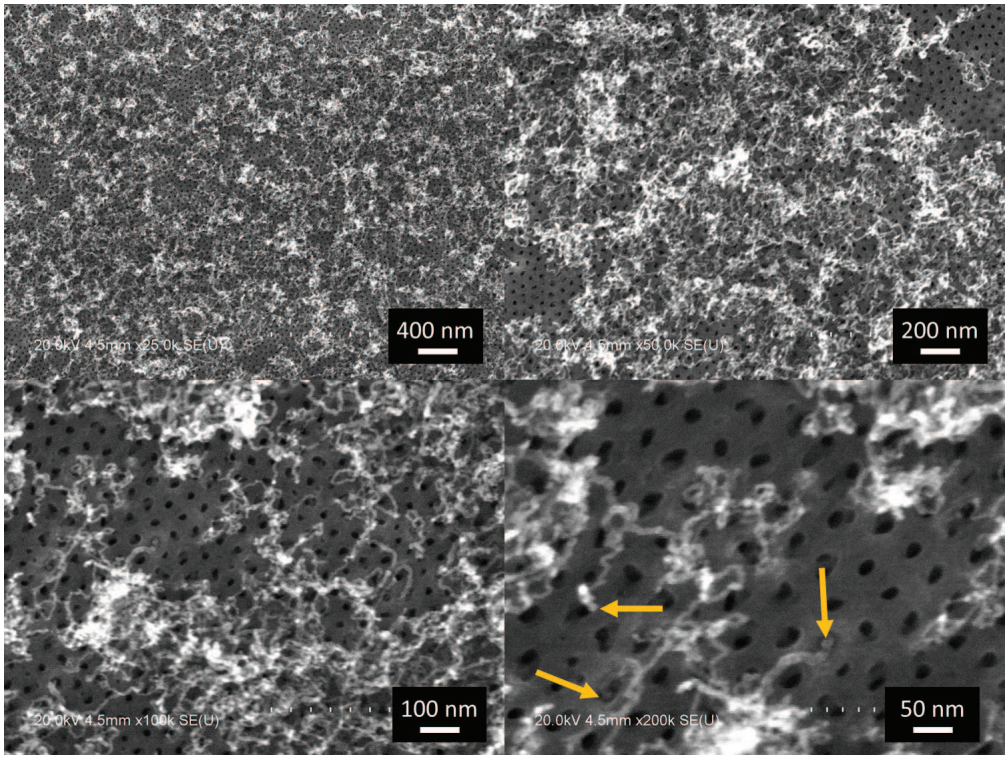

Figure 3.14: Top-views of a PAA after a 30 minute growth, performed at 500°C, H_2:CH_4 = 50:50 sccm, p = 50 mbar and P_f=180 W. Some CNTs protruding out of the PAA are visible in the bottom-right image (yellow arrows).

A similar sample, where no catalyst has been deposited before, has been inserted with the previous sample to act as a reference for the growth. As expected, no CNT nor any parasitic amorphous material has been found on the sample. This proves that the CNTs

observed in Figure 3.14 have been catalytically grown, and that they must be properly connected to the bottom of the pores, i.e where the Ni particles had been deposited.

3.3.4 TEM investigation and electron diffraction analysis

In order to investigate more deeply the as-formed SiNWs, and especially to get some information about their crystallinity, they were observed with a transmission electron microscope (TEM). The TEM observation requires some preliminary preparations. Contrary to a simple SEM observation, the samples have to be cut into thin sections ($<$ 100 nm) so that the incident electron beam goes through it. In our case, what we need to observe is already a few tens of nanometers thick, this step is therefore unnecessary. As in the SEM observation, an electron beam of a given energy impacts the sample (in our case, the typical energy of the electrons was 200 keV). The difference arises from the way the final image is composed. While the SEM pictures are formed from the secondary electrons extracted from the sample by the primary electron beam, the TEM pictures are based on a diffraction contrast and are formed directly from the incident electrons that, once diffracted, hit an electron-sensitive screen (scintillator), which emits a flash each time an electron impacts it. Below the sample, the objective (an electromagnetic lens) focuses the diffracted electrons and forms a real image (typically magnified 50x), which is intercepted by another set of electromagnetic lenses after the focal plane of the objective. These lenses magnify the image one more time and finally form this image on a fluorescent screen, so that it is directly observable with naked eye. A schematic comparison of both techniques is visible in Figure 3.15 (from [112]).

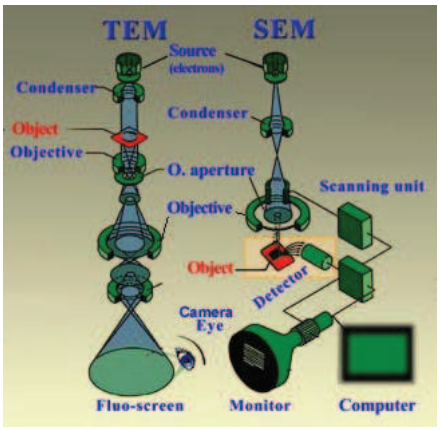

Figure 3.15: Comparative schematic drawing of TEM and SEM principle [112].

Another characterization technique, very often coupled to TEM observation, is the electron diffraction. All the TEMs provide this function, since it simply consists in recording the diffraction pattern of the electrons diffracted by the sample itself. In the imaging mode, the image is intercepted by the secondary set of lenses after the focal plane. In the diffraction mode, the set of lenses is simply laid out so as the image

formed on the screen corresponds to the focal plane of the objective, where diffracted electrons focus. Thus we can observe the diffraction pattern directly on the screen (see an example in Figure 3.16(c)). This pattern can reveal some essential information about the crystallinity of the observed sample. The electrons diffracted by a same family of crystallographic planes will converge in a sequence of spots, characteristic of these plane family. The identification of several spots can reveal which crystallographic planes of the observed sample diffract, and therefore reveal the crystallographic structure of the sample. If the sample is polycrystalline, i.e formed with same planes having different orientations, rings tend to form on the diffraction pattern. Finally, if the sample is amorphous, then no diffraction occurs since no crystallographic planes are present. This results in a blur, bright and circular pattern since every single atoms or molecules diffuse the incident electrons in their own way (an example is given in Figure 3.21).

After the growth, the SiNWs are still confined inside the PAA template and need to be extracted. The same method as in chapter 2 has been used to chemically etch the PAA (i.e a solution of H_3PO_4 and CrO_3) and thus liberate the NWs, that have been spread on a typical carbon-coated copper grid, commonly used to support nanostructures in TEM observation. As a first observation, we observed a nanowire grown at 540°C for 30 min (with $p = 2.5$ mbar, H_2:SiH_4 = 97.5:2.5 sccm and P_f=175 W). We first found that all the nanowires were about 40 nm in diameter, that is exactly the pore diameter they grew in. This shows that the catalyst size, contrary to growth on free surfaces, doesn't impact the nanowire diameter, since the latter is first limited by the pore walls (except of course if the catalyst is smaller than the pore diameter, in which case the resulting NW will be thinner than the pore). Figure 3.16(a) shows a nanowire with a polycrystalline structure, and reveals twins all across its length. All the observed crystalline SiNWs exhibited these kinds of features. Twinning is a defect that consists in a juxtaposition of two or more similar crystals, related to each other by a mirror symmetry about a {111} plane. The place where two crystals join is called twin boundary, and is the place where both crystal lattices are common. Twin boundaries are clearly visible in Figure 3.16(a) thanks to the high contrast between each neighbouring crystal (alternation of dark and bright areas). In this specific nanowire, it is found that the twins are of two types (see Figure 3.16(b)), which means that two different orientations with respect to the nanowire orientation have been found. The two kinds of twins are oriented one to each other with an angle of $\approx 70°$ (theoretically 70.53° according to twinning laws), about 45° with respect to the nanowire surface for the a-type twin, and about 20° for the b-type twin. These angles are conserved all along the the nanowire, and interestingly, we found several other SiNWs exhibiting the same twin arrangement when two kinds of twins were present, which proves that this arrangement is not due to chance. Nevertheless the twin orientations can vary between one nanowire to another, and no systematic study has been carried out in order to investigate the growth conditions-dependence on this feature.

An electron diffraction pattern (EDP) has been obtained from the nanowire shown in Figure 3.16(b) (see Figure 3.16(c)). The measurements of the angles and distances between the different spots allow to index them. In this case the spots have been identified as corresponding to the {111} and the {200} plane families, and the measured angles are

characteristic of the diamond cubic structure, that silicon takes in its crystalline phase. The vector product between a vector normal to the {111} family planes and a vector normal to the {200} family planes gives the zone axis, [110], which is the direction along which the nanowire is observed. One can notice the 70° disorientation between two spot families, that corresponds to the angle between the two families of {111} planes that are the mirror planes of the two kinds of twins in this wire. The presence of thin bright lines that join up the spots is due to the elongation of the spots, which occurs when the diffractive areas are very thin. A large monocrystal with no defect would normally lead to perfectly-defined spots. Figure 3.17 shows a magnification of Figure 3.16(a), and the corresponding oriented EDP. Once the EDP oriented, the blue dotted lines on the EDP, which are the perpendicular to the <111>* directions, are parallel to the twin boundaries shown on the TEM picture.

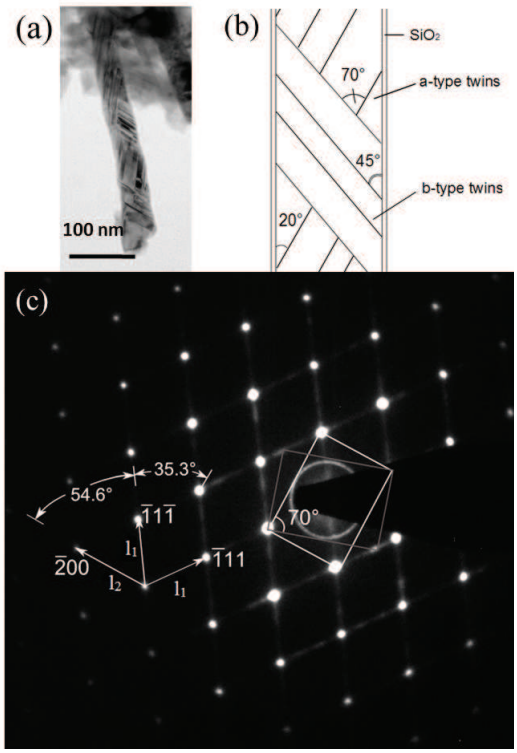

Figure 3.16: (a) and (b) TEM picture of a SiNW grown at 540°C. (b) Drawing of (a), angles between the two kinds of twins, and between the twins and the wire surface are reported. (c) Electron diffraction pattern of the wire shown in (a). The angles and distances measured to identify the crystallographic planes are shown.

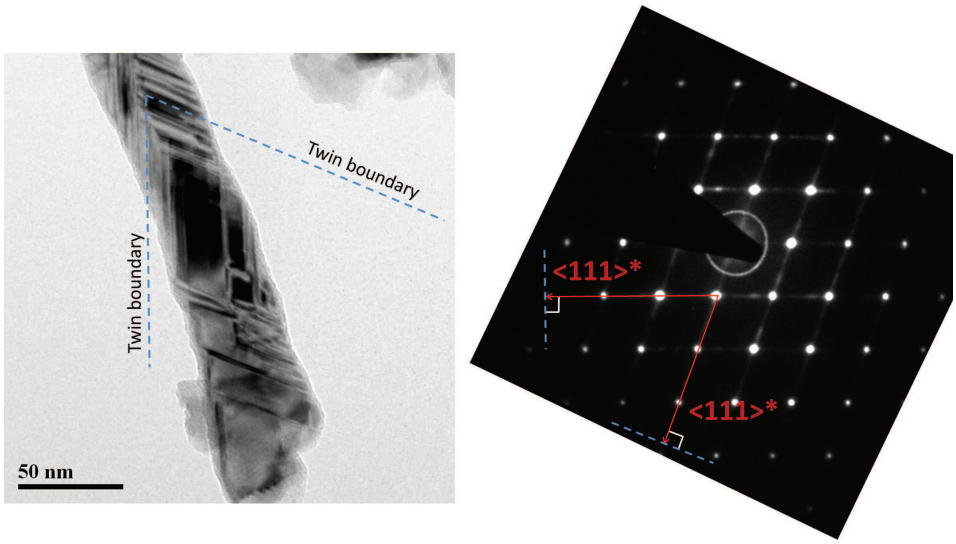

Figure 3.17: Left: high magnification TEM picture of the Figure 3.16(a) and right: corresponding oriented EDP with the construction lines used to determine the growth direction of the nanowire.

We could find some nanowires where one type of twin was predominant in a single wire, but we have never observed more than two types. An example is shown in Figure 3.18(a), where the twin boundaries are oriented in only one direction, except at the bottom tip of the nanowire. Here again the angle between the two types of twins is $\approx 70°$, the corresponding EDP is therefore very similar to the previous one. This nanowire has exactly the same properties as the one studied above, but it is interesting to understand where these "double spots", way brighter than in the previous EDP, come from. This EDP is actually the superimposition of the EDP of one type of twin and the EDP of the other one. By rotating the EDP shown in Figure 3.16(c) (where we can barely see the

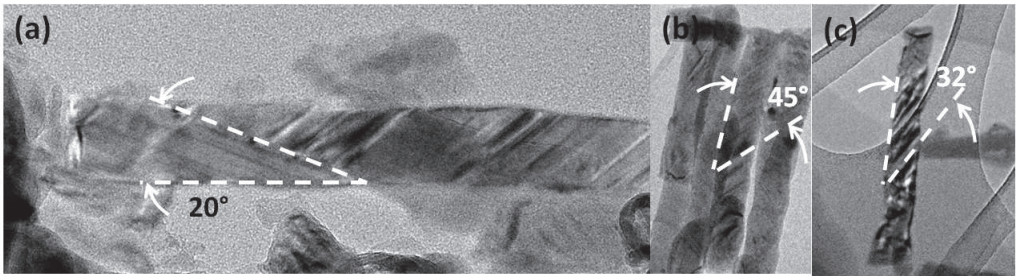

Figure 3.19: Three TEM pictures of SiNWs with highlighted twin orientations.

secondary spots) by 70° (the orientation of the two types of twins), we indeed find the EDP shown in 3.18.

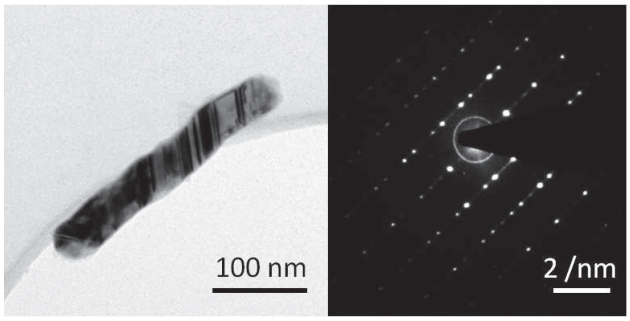

Figure 3.18: Left: a SiNW grown at 540°C and right: corresponding EDP revealing the diffraction planes.

SiNWs coming from a growth performed at 490°C for 1 h have also been observed. Very interestingly, we found some wires with one type of twins only exhibiting twins oriented 45° with respect to the nanowire, just like the ones grown at a higher temperature (Figure 3.19(b)). Moreover, the wires found with two kinds of twins also show an arrangement very similar as the ones described above, with a 20° tilt with respect to the wire surface for the b-type twins (Figure 3.19(a)). Nevertheless, these orientations, though encountered several times, were not systematic (see (Figure 3.19(c)) so no conclusion can be drawn yet. A dark particle found at the tip of a nanowire is suspected to be the particle that catalysed the nanowire growth (Figure 3.20(a)). A thin cap surrounding the catalyst is clearly visible and signs the Si incorporation on the catalyst surface during the growth. When used in the high-resolution mode, the TEM (HR-TEM) allows us to make out the Si atoms, well ordered in the wire stem (Figure 3.20(b) and to notice an ultra-thin layer (a few nm thick), very probably composed of silicon oxide, covering the nanowire surface.

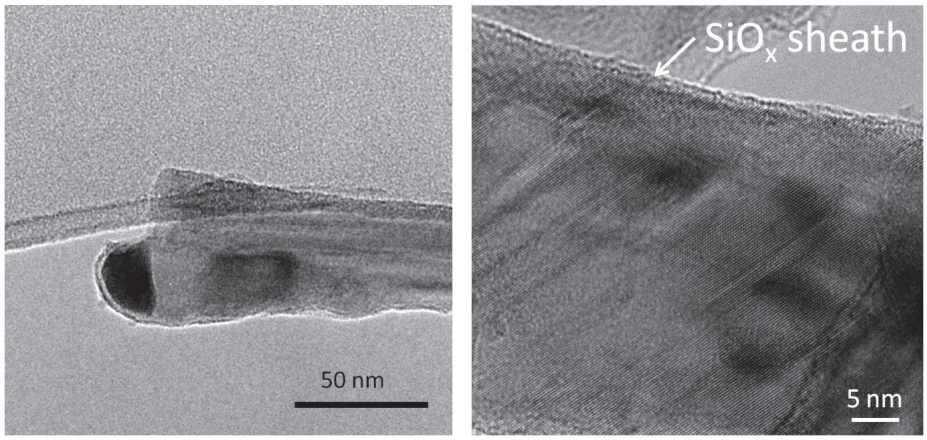

(a) (b)

Figure 3.20: (a) TEM picture of a SiNW exhibiting a catalyst particle at its tip (dark hemisphere) and (b) HR-TEM picture of a SiNW grown at 490°C.

Numerous EDP have been obtained from the Si nanostructures grown at 430°C; however no crystalline evidence has been highlighted. All the EDPs exhibited the characteristic blur, diffuse circles of an amorphous material, indicating as expected that no crystalline growth occurred at this temperature. The EDP in Figure 3.21 is shown as an illustration.

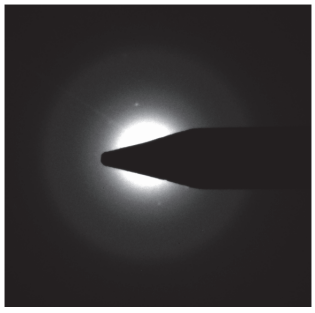

Figure 3.21: Electron diffraction pattern of amorphous SiNWs.

An interesting aspect of SiNW growth has been highlighted with the 580°C growth we carried out. We don't affirm that this only occurred in these conditions, but it's worthwhile to mention it. The SiNW shown in Figure 3.22 exhibits two separate parts in terms of contrast in the TEM image. They have been named "tail" and "head", respectively. The interesting point is that completely different EDPs have been obtained depending on the selected area of the wire, indicating a dramatic change in the growth mode in the middle of the growth.

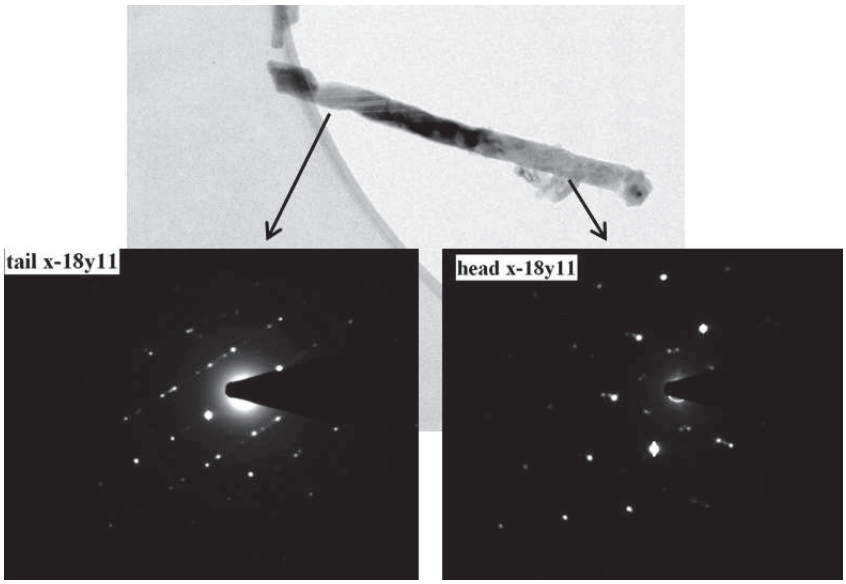

Figure 3.22: TEM picture of a SiNW exhibiting two distinct parts, with their corresponding EDPs.

We also studied the SiNTs, inevitably formed during the growth regardless of the growth conditions, from the deposition of a-Si on the pore walls. Their hollow structure was thus confirmed, consisting in a 40 nm in diameter cylinder, with 10 nm-thick a-Si walls as shown in Figure 3.23.

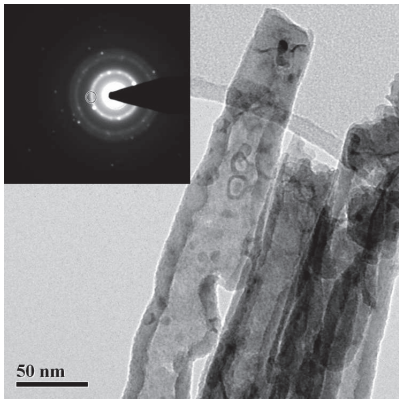

Figure 3.23: Amorphous SiNTs, formed from the a-Si deposition on the pore walls during the growth, with their corresponding EDP in the inset.

3.3.5 I(V) measurements (proof of concept)

As we managed to grow some SiNWs beyond the surface of the PAA template, an electrical measurement has become possible. Even if no large growth with one NW per pore has been achieved, such a measurement is nonetheless relevant, just to prove that a con-

tact had been created between the bottom of the structure and the surface, thanks to the NWs. No deep characterization of the as-grown NWs is planned. Indeed, since the efficiency of the growth was not so good, we couldn't know precisely the number of wires we connected. Despite the simplicity of these measurements, some interesting results have been found.

We used a classical two-probe system, connected to a Semiconductor Characterization System 4200 SCS, from Keithley, to perform I(V) measurements. Before all, and in order to make sure that we could rely on the alumina template as a good insulator, we performed some measurements on an empty sample, i.e on which no growth had been performed. We simply connected one probe onto the top of the PAA, the other one on the Si substrate, and applied a sweeping voltage between -5 V and 5 V, as drawn in Figure 3.24(a). As shown in Figure 3.24(b), the measured current appeared to be very low (in the order of $\approx 10^{-12}$A), and the slope corresponds to a resistance of $\approx 3.3.10^{12}$ Ω. This measurement has been done several times on different places of the same sample, and always gave similar results in terms of curve shape and order of magnitude, thus confirming the good insulating behaviour of the alumina consisting the PAA. Moreover, this indicates that though the PAA may contain some doping impurities, the latter don't contribute to any parasitic current.

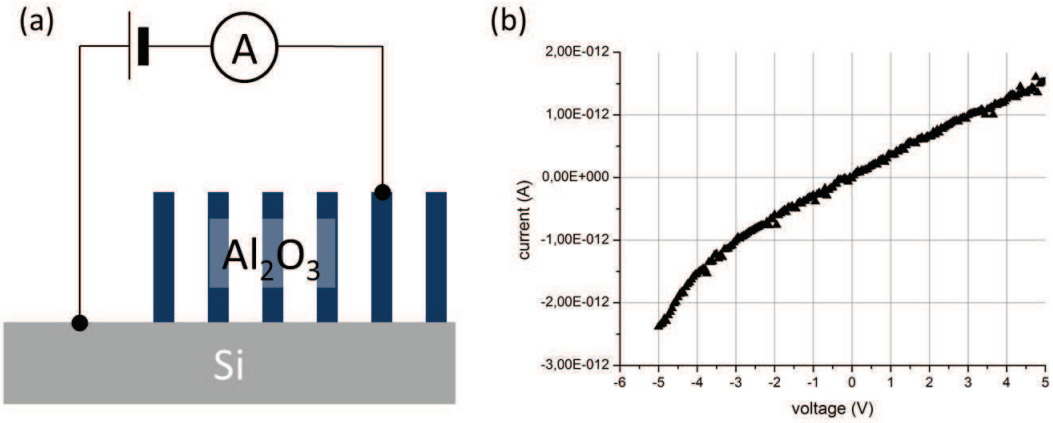

Figure 3.24: (a) Drawing of the principle of the electrical measurement and (b) I(V) curve for a measurement performed before the SiNW growth with two probes connected to the top of the PAA, and to the Si substrate, respectively, according to (a).

As a reference, we also measured the current through the silicon substrate, by contacting each probe to a different location on it. No matter how far the probes were from each other, we always got similar results concerning the current intensity. An example of an I(V) curve is shown in Figure 3.25 , which shows that the current is limited for voltages higher than (lower than) 2.3 V (-2.3 V). This high current is of course due to the doping of the substrates we used, and shows that the substrate is not a limiting element for the current in our measurements.

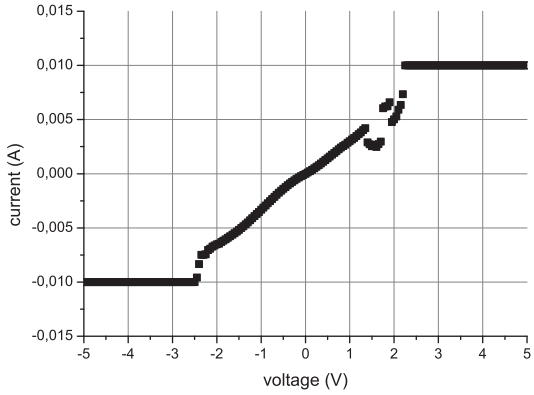

Figure 3.25: I(V) curve of a Si substrate, both probes connected to it. Our Keithley system saturates for currents superior to 10 mA.

Then we carried out the measurements on a similar sample, on which SiNW growth has been performed for 40 min around 450°C, with H_2:SiH_4 = 90:10 sccm at 5 mbar. Those conditions were found to lead to both SiNWs and a-Si deposit, but with the advantage that a few SiNWs protruded out from the PAA (see Figures 3.26(a) and 3.26(b)). The principle of the measurement was the same as with the empty sample, except we expected the probe to contact some SiNWs on the top of the PAA, thus creating a contact between the silicon substrate and the top of the sample. The corresponding I(V) curve is visible in Figure 3.26(e), and clearly exhibits some dramatic changes, starting with the magnitude of the current, which increased 8 orders of magnitude compared to the previous sample, proving that SiNWs and/or SiNTs effectively act as a path between the probe on the PAA and the silicon substrate. Besides, the I(V) curve exhibits a typically diode-like shape, which must be due to the nonohmic contact between the metallic probe and the semiconducting silicon of the NWs, which forms a Schottky junction. As can clearly be seen on Figures 3.26(c) and 3.26(d), the material present inside the PAA is of several nature. Thanks to the removal of the PAA, we can see both plain nanowires and hollow nanotubes inside the same sample, kept all together thanks to an a-Si crust, already observed before. We even realized that almost all the pores must contain such nanotubes, and only a few of them contain catalytically-grown SiNWs. Indeed, most of the observed structures are the exact height of the PAA (sign of a deposit on the PAA walls), whereas very few nanowires are higher.

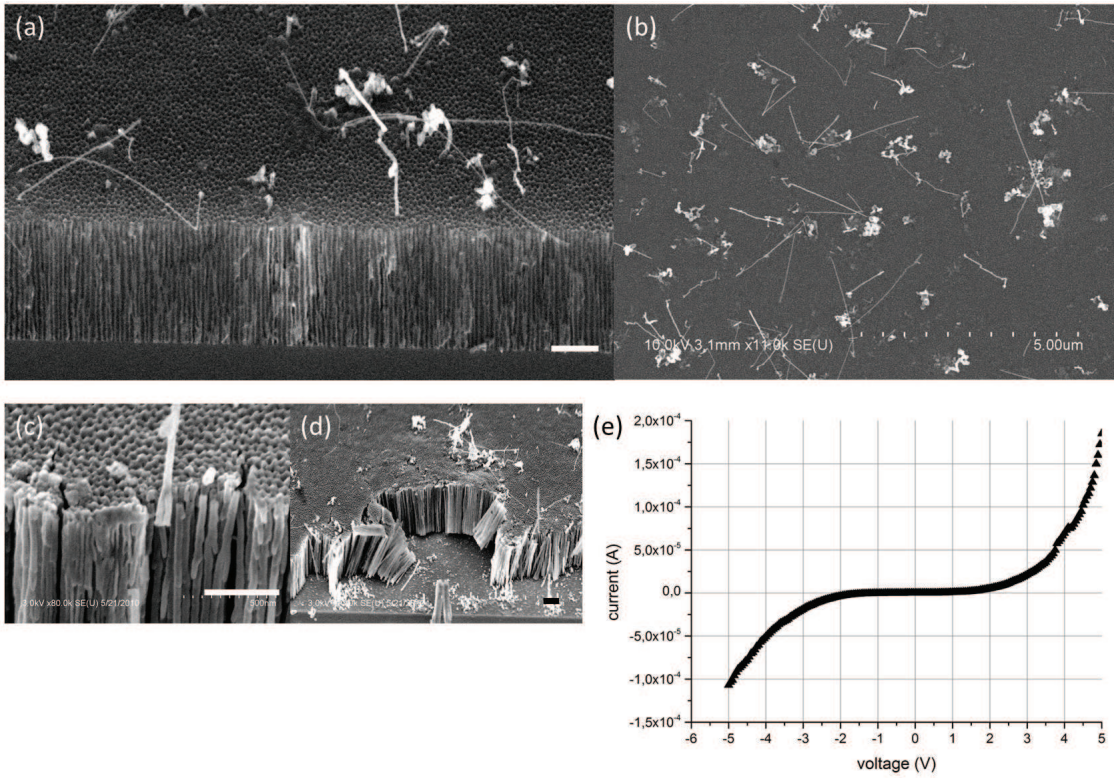

Figure 3.26: (a) SEM cross-section and (b) top view of a PAA template after a SiNW growth at 450°C, 5 mbar and with H_2:SiH_4 = 90:10 sccm. (c) and (d) Tilted views of the same sample after PAA removal. (e) I(V) curve for a measurement performed after the SiNW growth with two probes connected to the top of the PAA, and the Si substrate, respectively. Scale bars in (a), (c) and (d) are 400 nm.

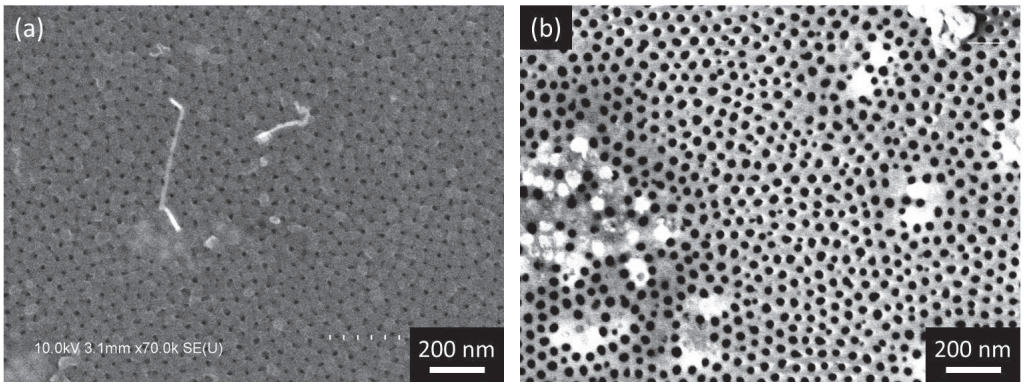

Figure 3.27: SEM top views of a PAA sample after a SiNW growth (a) before and (b) after the a-Si crust etching.

The same ICP etching as described in p.81 has been performed on a part of the sample,

in order to partially remove the a-Si crust on the top of the surface. The pictures in Figure 3.27 show a top view of the surface before and after the etching, clearly demonstrating that amorphous silicon clogged the pores. Some I(V) measurement has been performed again, but too many different results prevent us from concluding about the influence of what had been etched away. Depending on the place where the micro-probe was connected, the current was indeed either the same as before the etching, or several orders of magnitude below.

This study has shown that a different electrical behaviour can be expected by comparing PAA before and after SiNW growth. We have thus checked and confirmed that the PAA template is a good insulator and we have clearly shown that a dramatic increase in the current intensity is measured between the top of the PAA and the Si substrate, proving that a semiconducting path has been created by performing the SiNW growth.

3.4 Conclusion

1D nanostructures have such a potential in so many applications, that their behaviour and growth mechanisms deserve to be understood thoroughly if one wants to use them as building blocks in electronic nanodevices. Since the 90s, a lot of synthesis methods have seen the light and have given birth to a wide variety of nanostructures, as mentioned at the beginning of this chapter. The next step on our way to fabricate a vertical 1D nanostructure-based FET was to grow a single nanowire or a single nanotube in each pore. Here, we have brought a proof of concept by growing SiNWs and CNTs inside PAA, which is promising for the continuation. The influence of the growth conditions of our HWCVD reactor has been investigated in order to find optimized conditions for proper growth. It has been found that SiNWs, thanks to the help of atomic hydrogen, could be grown inside the pores with a limited formation of amorphous silicon, and that some nanowires even protruded out of the PAA. We also performed successful CNT growths in PAA. However, we couldn't reach the "one nanostructure per pore" level, mainly because of a lack of control over the catalyst deposition. A TEM investigation allowed to affirm that the some of the as-formed SiNWs were crystalline, and exhibited a twinned structure. We then carried out an electron diffraction study to determine their growth direction. Finally, some basic electrical measurements provided evidence about the connection between the top of the PAA membrane and the Si substrate, brought by the SiNW growth. Though these results can be improved, they constitute an important basis to continue our work towards the fabrication of a vertical FET. What happens next consists of the fabrication of a porous structure, which must be able both to receive 1D nanostructures as well as to provide electrical features to contact them. This is the subject of the fourth chapter.

Bibliography

[1] V. Schmidt, J. V. Wittemann, and U. Gösele, "Growth, thermodynamics, and electrical properties of silicon nanowires," *Chemical reviews*, vol. 110, pp. 361–388, Jan. 2010. PMID: 20070117.

[2] V. Schmidt, J. V. Wittemann, S. Senz, and U. Gösele, "Silicon nanowires: A review on aspects of their growth and their electrical properties," *Advanced Materials*, vol. 21, no. 25-26, pp. 2681–2702, 2009.

[3] M. Shao, D. D. D. Ma, and S.-T. Lee, "Silicon nanowires – synthesis, properties, and applications," *European Journal of Inorganic Chemistry*, vol. 2010, pp. 4264–4278, Aug. 2010.

[4] M. Hernández-Vélez, "Nanowires and 1D arrays fabrication: An overview," *Thin Solid Films*, vol. 495, pp. 51–63, Jan. 2006.

[5] Y. Xia, P. Yang, Y. Sun, Y. Wu, B. Mayers, B. Gates, Y. Yin, F. Kim, and H. Yan, "One-dimensional nanostructures: Synthesis, characterization, and applications," *Advanced Materials*, vol. 15, pp. 353–389, Mar. 2003.

[6] I. Park, Z. Li, A. P. Pisano, and R. S. Williams, "Top-down fabricated silicon nanowire sensors for real-time chemical detection," *Nanotechnology*, vol. 21, p. 015501, Jan. 2010.

[7] G. Pennelli, "Top down fabrication of long silicon nanowire devices by means of lateral oxidation," *Microelectronic Engineering*, vol. 86, pp. 2139–2143, Nov. 2009.

[8] K.-N. Lee, S.-W. Jung, K.-S. Shin, W.-H. Kim, M.-H. Lee, and W.-K. Seong, "Fabrication of suspended silicon nanowire arrays," *Small*, vol. 4, pp. 642–648, Apr. 2008.

[9] S. Feste, J. Knoch, D. Buca, and S. Mantl, "Fabrication of uniaxially strained silicon nanowires," *Thin Solid Films*, vol. 517, pp. 320–322, Nov. 2008.

[10] S. Chen, J. G. Bomer, W. G. van der Wiel, E. T. Carlen, and A. van den Berg, "Top-down fabrication of sub-30 nm monocrystalline silicon nanowires using conventional microfabrication," *ACS Nano*, vol. 3, no. 11, pp. 3485–3492, 2009.

[11] Y. Sun, R. A. Graff, M. S. Strano, and J. A. Rogers, "TopDown fabrication of semiconductor nanowires with alternating structures along their longitudinal and transverse axes," *Small*, vol. 1, pp. 1052–1057, Sept. 2005.

[12] D. Whang, S. Jin, and C. M. Lieber, "Nanolithography using hierarchically assembled nanowire masks," *Nano Lett.*, vol. 3, no. 7, pp. 951–954, 2003.

[13] N. A. Melosh, A. Boukai, F. Diana, B. Gerardot, A. Badolato, P. M. Petroff, and J. R. Heath, "Ultrahigh-density nanowire lattices and circuits," *Science*, vol. 300, pp. 112–115, Apr. 2003.

[14] B. Hausmann, M. Khan, T. Babinec, Y. Zhang, K. Martinick, M. McCutcheon, P. Hemmer, and M. Loncar, "Fabrication of diamond nanowires for quantum information processing applications," *arXiv:0908.0352*, Aug. 2009.

[15] C.-M. Hsu, S. T. Connor, M. X. Tang, and Y. Cui, "Wafer-scale silicon nanopillars and nanocones by Langmuir–Blodgett assembly and etching," *Applied Physics Letters*, vol. 93, pp. 133109–133109–3, Oct. 2008.

[16] N. Geyer, U. Gösele, Z. Huang, and B. Fuhrmann, "Sub-20 nm si-ge superlattice nanowires by metal-assisted etching," *Nano Letters*, vol. 9, no. 9, pp. 3106–3110, 2009.

[17] S. Iijima, "Helical microtubules of graphitic carbon," *Nature*, vol. 354, no. 6348, pp. 56–58, 1991.

[18] N. Koprinarov, "Silicon nanowires and whiskers obtained by arc discharge," *Journal of physics. Conference series*, vol. 113, p. 12007, Jan. 2008.

[19] N. Koprinarov, M. Marinov, and M. Konstantinova, "An arc discharge by closely situated electrodes for synthesis of nanostructures," *Solid State Phenomena*, vol. 159, pp. 181–184, Jan. 2010.

[20] V. Pokropivny and M. Kasumov, "Synthesis and growth mechanism of zinc oxide nanostructures in arc discharge," *Technical Physics Letters*, vol. 33, no. 1, pp. 44–47, 2007.

[21] J. D. Holmes, "Control of thickness and orientation of solution-grown silicon nanowires," *Science*, vol. 287, pp. 1471–1473, Feb. 2000.

[22] H.-Y. Tuan, D. C. Lee, T. Hanrath, and B. A. Korgel, "Catalytic solid-phase seeding of silicon nanowires by nickel nanocrystals in organic solvents," *Nano Lett.*, vol. 5, no. 4, pp. 681–684, 2005.

[23] H.-Y. Tuan, A. Ghezelbash, and B. A. Korgel, "Silicon nanowires and silica nanotubes seeded by copper nanoparticles in an organic solvent," *Chem. Mater.*, vol. 20, no. 6, pp. 2306–2313, 2008.

[24] T. J. Trentler, K. M. Hickman, S. C. Goel, A. M. Viano, P. C. Gibbons, and W. E. Buhro, "Solution-liquid-solid growth of crystalline III-V semiconductors: An analogy to vapor-liquid-solid growth," *Science*, vol. 270, pp. 1791–1794, Dec. 1995.

[25] L. Schubert, P. Werner, N. D. Zakharov, G. Gerth, F. M. Kolb, L. Long, U. Gösele, and T. Y. Tan, "Silicon nanowhiskers grown on 111Si substrates by molecular-beam epitaxy," *Applied Physics Letters*, vol. 84, pp. 4968–4970, May 2004.

[26] E. Calleja, M. A. Sánchez-García, F. J. Sánchez, F. Calle, F. B. Naranjo, E. Muñoz, U. Jahn, and K. Ploog, "Luminescence properties and defects in GaN nanocolumns grown by molecular beam epitaxy," *Physical Review B*, vol. 62, pp. 16826–16834, Dec. 2000.

[27] O. Landré, V. Fellmann, P. Jaffrennou, C. Bougerol, H. Renevier, A. Cros, and B. Daudin, "Molecular beam epitaxy growth and optical properties of AlN nanowires," *Applied Physics Letters*, vol. 96, pp. 061912–061912–3, Feb. 2010.

[28] T. Stoica, R. Meijers, R. Calarco, T. Richter, and H. Lüth, "MBE growth optimization of InN nanowires," *Journal of Crystal Growth*, vol. 290, pp. 241–247, Apr. 2006.

[29] A. P. Vajpeyi, A. O. Ajagunna, K. Tsagaraki, M. Androulidaki, and A. Georgakilas, "InGaN nanopillars grown on silicon substrate using plasma assisted molecular beam epitaxy," *Nanotechnology*, vol. 20, p. 325605, Aug. 2009.

[30] J. Sadowski, P. Dluzewski, and J. Kanski, "Autocatalytic MBE growth of GaAs nanowires on oxidized si(100)," *arXiv:0812.2453*, Dec. 2008.

[31] A. Fontcuberta i Morral, C. Colombo, G. Abstreiter, J. Arbiol, and J. R. Morante, "Nucleation mechanism of gallium-assisted molecular beam epitaxy growth of gallium arsenide nanowires," *Applied Physics Letters*, vol. 92, pp. 063112–063112–3, Feb. 2008.

[32] B. Mandl, J. Stangl, T. Mårtensson, A. Mikkelsen, J. Eriksson, L. S. Karlsson, G. Bauer, L. Samuelson, and W. Seifert, "Au-free epitaxial growth of InAs nanowires," *Nano Lett.*, vol. 6, no. 8, pp. 1817–1821, 2006.

[33] X. Cai, A. Djurišić, and M. Xie, "GaN nanowires: CVD synthesis and properties," *Thin Solid Films*, vol. 515, pp. 984–989, Nov. 2006.

[34] B. Geng, T. Xie, X. Peng, Y. Lin, X. Yuan, G. Meng, and L. Zhang, "Large-scale synthesis of ZnO nanowires using a low-temperature chemical route and their photoluminescence properties," *Applied Physics A: Materials Science & Processing*, vol. 77, no. 3, pp. 363–366, 2003.

[35] H. Y. Dang, J. Wang, and S. S. Fan, "The synthesis of metal oxide nanowires by directly heating metal samples in appropriate oxygen atmospheres," *Nanotechnology*, vol. 14, pp. 738–741, July 2003.

[36] S. Hofmann, R. Sharma, C. Ducati, G. Du, C. Mattevi, C. Cepek, M. Cantoro, S. Pisana, A. Parvez, F. Cervantes-Sodi, A. C. Ferrari, R. Dunin-Borkowski, S. Lizzit, L. Petaccia, A. Goldoni, and J. Robertson, "In situ observations of catalyst dynamics during surface-bound carbon nanotube nucleation," *Nano Lett.*, vol. 7, no. 3, pp. 602–608, 2007.

[37] S. Fan, L. Liu, and M. Liu, "Monitoring the growth of carbon nanotubes by carbon isotope labelling," *Nanotechnology*, vol. 14, pp. 1118–1123, Oct. 2003.

[38] X. Li, A. Cao, Y. J. Jung, R. Vajtai, and P. M. Ajayan, "Bottom-up growth of carbon nanotube multilayers: unprecedented growth," *Nano Lett.*, vol. 5, no. 10, pp. 1997–2000, 2005.

[39] R. Schropp, C. v. d. Werf, V. Verlaan, J. Rath, and H. Li, "Ultrafast deposition of silicon nitride and semiconductor silicon thin films by hot wire chemical vapor deposition," *Thin solid films*, vol. in press, 2009.

[40] I. T. Martin, C. W. Teplin, P. Stradins, M. Landry, M. Shub, R. C. Reedy, B. To, J. V. Portugal, and J. T. Mariner, "High rate hot-wire chemical vapor deposition of silicon thin films using a stable TaC covered graphite filament," *Thin Solid Films*, vol. 519, pp. 4585–4588, May 2011.

[41] N. P. Meshram, A. Kumbhar, and R. Dusane, "Silicon nanowire growth on glass substrates using hot wire chemical vapor deposition," *Thin Solid Films*, vol. 519, pp. 4609–4612, May 2011.

[42] J. Thiesen, E. Iwaniczko, K. M. Jones, A. Mahan, and R. Crandall, "Growth of epitaxial silicon at low temperatures using hot-wire chemical vapor deposition," *Applied Physics Letters*, vol. 75, pp. 992–994, Aug. 1999.

[43] F. Z. Bouanis, L. Baraton, V. Huc, D. Pribat, and C. S. Cojocaru, "High-quality single-walled carbon nanotubes synthesis by hot filament CVD on ru nanoparticle catalyst," *Thin Solid Films*, vol. 519, pp. 4594–4597, May 2011.

[44] K.-H. Kim, E. Lefeuvre, M. Châtelet, D. Pribat, and C. S. Cojocaru, "Laterally organized carbon nanotube arrays based on hot-filament chemical vapor deposition," *Thin Solid Films*, vol. 519, pp. 4598–4602, May 2011.

[45] E. Lefeuvre, K. Kim, Z. He, J.-L. Maurice, M. Châtelet, D. Pribat, and C. Cojocaru, "Optimization of organized silicon nanowires growth inside porous anodic alumina template using hot wire chemical vapor deposition process," *Thin Solid Films*, vol. 519, pp. 4603–4608, May 2011.

[46] T. Guo, P. Nikolaev, A. G. Rinzler, D. Tomanek, D. T. Colbert, and R. E. Smalley, "Self-assembly of tubular fullerenes," *J. Phys. Chem.*, vol. 99, no. 27, pp. 10694–10697, 1995.

[47] T. Guo, P. Nikolaev, A. Thess, D. Colbert, and R. Smalley, "Catalytic growth of single-walled manotubes by laser vaporization," *Chemical Physics Letters*, vol. 243, pp. 49–54, Sept. 1995.

[48] A. M. Morales, "A laser ablation method for the synthesis of crystalline semiconductor nanowires," *Science*, vol. 279, pp. 208–211, Jan. 1998.

[49] G. W. Zhou, Z. Zhang, Z. G. Bai, S. Q. Feng, and D. P. Yu, "Transmission electron microscopy study of si nanowires," *Applied Physics Letters*, vol. 73, pp. 677–679, Aug. 1998.

[50] D. P. Yu, X. S. Sun, C. S. Lee, I. Bello, S. T. Lee, H. D. Gu, K. M. Leung, G. W. Zhou, Z. F. Dong, and Z. Zhang, "Synthesis of boron nitride nanotubes by means of excimer laser ablation at high temperature," *Applied Physics Letters*, vol. 72, pp. 1966–1968, Apr. 1998.

[51] Y. H. Tang, T. K. Sham, A. Jürgensen, Y. F. Hu, C. S. Lee, and S. T. Lee, "Phosphorus-doped silicon nanowires studied by near edge x-ray absorption fine structure spectroscopy," *Applied Physics Letters*, vol. 80, pp. 3709–3711, May 2002.

[52] R. S. Wagner and W. C. Ellis, "VAPOR-LIQUID-SOLID MECHANISM OF SINGLE CRYSTAL GROWTH," *Applied Physics Letters*, vol. 4, no. 5, p. 89, 1964.

[53] P. Rudolph, "Highly anisotropic crystals. series MSMR (Material science of minerals and rocks). d. reidel publishing company, dordrecht, boston, lancaster, tokyo in copublication with terra scientific publishing company, tokyo, 1987. 394 seiten mit 100 abbildungen und 21 tabellen, sachwörterverzeichnis, substanzverzeichnis, preis 230,— dfl., 98,— US dollar. ISBN 9027721726," *Crystal Research and Technology*, vol. 22, pp. 1120–1120, Sept. 1987.

[54] R. Baker, "Catalytic growth of carbon filaments," *Carbon*, vol. 27, no. 3, pp. 315–323, 1989.

[55] H. Dai, A. G. Rinzler, P. Nikolaev, A. Thess, D. T. Colbert, and R. E. Smalley, "Single-wall nanotubes produced by metal-catalyzed disproportionation of carbon monoxide," *Chemical Physics Letters*, vol. 260, pp. 471–475, Sept. 1996.

[56] Z. F. Ren, Z. P. Huang, J. W. Xu, J. H. Wang, P. Bush, M. P. Siegal, and P. N. Provencio, "Synthesis of large arrays of well-aligned carbon nanotubes on glass," *Science*, vol. 282, pp. 1105–1107, June 1998.

[57] C. J. Lee, D. W. Kim, T. J. Lee, Y. C. Choi, Y. S. Park, Y. H. Lee, W. B. Choi, N. S. Lee, G.-S. Park, and J. M. Kim, "Synthesis of aligned carbon nanotubes using thermal chemical vapor deposition," *Chemical Physics Letters*, vol. 312, pp. 461–468, Oct. 1999.

[58] J.-B. Park, Y.-S. Cho, S.-Y. Hong, K.-S. Choi, D. Kim, S.-Y. Choi, S.-D. Ahn, Y.-H. Song, J.-H. Lee, and K.-I. Cho, "Cross-sectional transmission electron microscopy of carbon nanotubes–catalyst–substrate heterostructure using a novel method for specimen preparation," *Thin Solid Films*, vol. 415, pp. 78–82, Aug. 2002.

[59] G. S. Choi, Y. S. Cho, S. Y. Hong, J. B. Park, K. H. Son, and D. J. Kim, "Carbon nanotubes synthesized by ni-assisted atmospheric pressure thermal chemical vapor deposition," *Journal of Applied Physics*, vol. 91, pp. 3847–3854, Mar. 2002.

[60] M. S. Al-Ruqeishi, R. M. Nor, Y. M. Amin, K. Al-Azri, M. Rusop, and T. Soga, "Amorphous SiOx nanowires and aligned nano-cakes: The growth mechanism and photoluminescence," pp. 414–419, AIP, 2009.

[61] S. Y. Pung, C. C. Tee, K. L. Choy, and X. H. Hou, "Growth mechanism of au-catalyzed zno nanowires: VLS or VS-VLS?," *Advanced Materials Research*, vol. 364, pp. 333–337, Oct. 2011.

[62] F. Liu, J. Tian, L. Bao, T. Yang, C. Shen, X. Lai, Z. Xiao, W. Xie, S. Deng, J. Chen, J. She, N. Xu, and H. Gao, "Fabrication of vertically aligned SingleCrystalline boron nanowire arrays and investigation of their FieldEmission behavior," *Advanced Materials*, vol. 20, pp. 2609–2615, May 2008.

[63] N. Chopra, B. Hu, and B. J. Hinds, "Selective growth and kinetic study of copper oxide nanowires from patterned thin-film multilayer structures," *Journal of Materials Research*, vol. 22, no. 10, pp. 2691–2699, 2007.

[64] N. H. Quang and D.-H. Kim, "Control of growth mode of multiwalled carbon nanotubes," *Journal of Physics: Conference Series*, vol. 187, p. 012065, Sept. 2009.

[65] M. Kumar, "Carbon nanotube synthesis and growth mechanism," in *Carbon Nanotubes - Synthesis, Characterization, Applications* (S. Yellampalli, ed.), InTech, July 2011.

[66] S. Kodambaka, J. Tersoff, M. C. Reuter, and F. M. Ross, "Germanium nanowire growth below the eutectic temperature," *Science*, vol. 316, pp. 729–732, Apr. 2007.

[67] Y. Wong, M. Yahaya, M. Mat Salleh, and B. Yeop Majlis, "Controlled growth of silicon nanowires synthesized via solid–liquid–solid mechanism," *Science and Technology of Advanced Materials*, vol. 6, pp. 330–334, Apr. 2005.

[68] H. Yan, Y. Xing, Q. Hang, D. Yu, Y. Wang, J. Xu, Z. Xi, and S. Feng, "Growth of amorphous silicon nanowires via a solid–liquid–solid mechanism," *Chemical Physics Letters*, vol. 323, pp. 224–228, June 2000.

[69] D. Yu, Y. Xing, Q. Hang, H. Yan, J. Xu, Z. Xi, and S. Feng, "Controlled growth of oriented amorphous silicon nanowires via a solid–liquid–solid (SLS) mechanism," *Physica E: Low-dimensional Systems and Nanostructures*, vol. 9, pp. 305–309, Feb. 2001.

[70] L. Yu, P.-J. Alet, G. Picardi, and P. Roca i Cabarrocas, "An in-plane solid-liquid-solid growth mode for self-avoiding lateral silicon nanowires," *Physical Review Letters*, vol. 102, p. 125501, Mar. 2009.

[71] M. Paulose, O. K. Varghese, and C. A. Grimes, "Synthesis of gold-silica composite nanowires through solid-liquid-solid phase growth," *Journal of nanoscience and nanotechnology*, vol. 3, pp. 341–346, Aug. 2003. PMID: 14598450.

[72] Y. Xing, Q. Hang, H. Yan, H. Pan, J. Xu, D. Yu, Z. Xi, Z. Xue, and S. Feng, "Solid–liquid–solid (SLS) growth of coaxial nanocables: silicon carbide sheathed with silicon oxide," *Chemical Physics Letters*, vol. 345, pp. 29–32, Sept. 2001.

[73] J. Westwater, D. P. Gosain, S. Tomiya, S. Usui, and H. Ruda, "Growth of silicon nanowires via gold/silane vapor–liquid–solid reaction," *Journal of Vacuum Science & Technology B: Microelectronics and Nanometer Structures*, vol. 15, pp. 554–557, May 1997.

[74] J. Kikkawa, Y. Ohno, and S. Takeda, "Growth rate of silicon nanowires," *Applied Physics Letters*, vol. 86, pp. 123109–123109–3, Mar. 2005.

[75] S. Akhtar, K. Usami, Y. Tsuchiya, H. Mizuta, and S. Oda, "Vapor–Liquid–Solid growth of small- and uniform-diameter silicon nanowires at low temperature from Si2H6," *Applied Physics Express*, vol. 1, p. 014003, 2008.

[76] J. B. Hannon, S. Kodambaka, F. M. Ross, and R. M. Tromp, "The influence of the surface migration of gold on the growth of silicon nanowires," *Nature*, vol. 440, pp. 69–71, Jan. 2006.

[77] V. Schmidt, S. Senz, and U. Gösele, "Diameter-dependent growth direction of epitaxial silicon nanowires," *Nano Letters*, vol. 5, pp. 931–935, May 2005. PMID: 15884897.

[78] Y. Wu, Y. Cui, L. Huynh, C. J. Barrelet, D. C. Bell, and C. M. Lieber, "Controlled growth and structures of molecular-scale silicon nanowires," *Nano Lett.*, vol. 4, no. 3, pp. 433–436, 2004.

[79] E. Givargizov, "Fundamental aspects of VLS growth," *Journal of Crystal Growth*, vol. 31, pp. 20–30, Dec. 1975.

[80] F. Dhalluin, T. Baron, P. Ferret, B. Salem, P. Gentile, and J. C. Harmand, "Silicon nanowires: Diameter dependence of growth rate and delay in growth," *Applied Physics Letters*, vol. 96, pp. 133109–133109–3, Apr. 2010.

[81] J. Weyher, "Some notes on the growth kinetics and morphology of VLS silicon crystals grown with platinum and gold as liquid-forming agents," *Journal of Crystal Growth*, vol. 43, pp. 235–244, Mar. 1978.

[82] S. Kodambaka, J. Tersoff, M. C. Reuter, and F. M. Ross, "Diameter-independent kinetics in the vapor-liquid-solid growth of si nanowires," *Physical Review Letters*, vol. 96, p. 096105, Mar. 2006.

[83] V. Schmidt, S. Senz, and U. Gösele, "Diameter dependence of the growth velocity of silicon nanowires synthesized via the vapor-liquid-solid mechanism," *Physical Review B*, vol. 75, p. 045335, Jan. 2007.

[84] M.-K. Li, D.-Z. Wang, Y.-W. Ding, X.-Y. Guo, S. Ding, and H. Jin, "Morphology and field emission from ZnO nanowire arrays synthesized at different temperature," *Materials Science and Engineering: A*, vol. 452–453, pp. 417–421, Apr. 2007.

[85] R. Saito, M. Fujita, G. Dresselhaus, and M. S. Dresselhaus, "Electronic structure of chiral graphene tubules," *Applied Physics Letters*, vol. 60, pp. 2204–2206, May 1992.

[86] B. Kitiyanan, W. Alvarez, J. Harwell, and D. Resasco, "Controlled production of single-wall carbon nanotubes by catalytic decomposition of CO on bimetallic Co–Mo catalysts," *Chemical Physics Letters*, vol. 317, pp. 497–503, Feb. 2000.

[87] A. Rinzler, J. Liu, H. Dai, P. Nikolaev, C. Huffman, F. Rodríguez-Macías, P. Boul, A. Lu, D. Heymann, D. Colbert, R. Lee, J. Fischer, A. Rao, P. Eklund, and R. Smalley, "Large-scale purification of single-wall carbon nanotubes: process, product, and characterization," *Applied Physics A: Materials Science & Processing*, vol. 67, no. 1, pp. 29–37, 1998.

[88] C. Journet, W. K. Maser, P. Bernier, A. Loiseau, M. L. d. l. Chapelle, S. Lefrant, P. Deniard, R. Lee, and J. E. Fischer, "Large-scale production of single-walled carbon nanotubes by the electric-arc technique," *Nature*, vol. 388, pp. 756–758, Aug. 1997.

[89] M. P. Zach, "Molybdenum nanowires by electrodeposition," *Science*, vol. 290, pp. 2120–2123, Dec. 2000.

[90] M. Walther, E. Kapon, J. Christen, D. M. Hwang, and R. Bhat, "Carrier capture and quantum confinement in GaAs/AlGaAs quantum wire lasers grown on vgrooved substrates," *Applied Physics Letters*, vol. 60, pp. 521–523, Feb. 1992.

[91] E. Olson, G. C. Spalding, A. M. Goldman, and M. J. Rooks, "New method for fabricating ultranarrow metallic wires," *Applied Physics Letters*, vol. 65, pp. 2740–2742, Nov. 1994.

[92] G. Fasol, "APPLIED PHYSICS: nanowires: Small is beautiful," *Science*, vol. 280, pp. 545–546, Apr. 1998.

[93] L. J. Lauhon, M. S. Gudiksen, D. Wang, and C. M. Lieber, "Epitaxial core|[ndash]|shell and core|[ndash]|multishell nanowire heterostructures," *Nature*, vol. 420, pp. 57–61, Nov. 2002.

[94] Y. Zhang and H. Dai, "Formation of metal nanowires on suspended single-walled carbon nanotubes," *Applied Physics Letters*, vol. 77, pp. 3015–3017, Nov. 2000.

[95] E. Braun, Y. Eichen, U. Sivan, and G. Ben-Yoseph, "DNA-templated assembly and electrode attachment of a conducting silver wire," *Nature*, vol. 391, pp. 775–778, Feb. 1998.

[96] S.-H. Jeong, H.-Y. Hwang, S.-K. Hwang, and K.-H. Lee, "Carbon nanotubes based on anodic aluminum oxide nano-template," *Carbon*, vol. 42, no. 10, pp. 2073–2080, 2004.

[97] J. Li, C. Papadopoulos, and J. Xu, "Nanoelectronics: Growing y-junction carbon nanotubes," *Nature*, vol. 402, pp. 253–254, Nov. 1999.

[98] J. Li, C. Papadopoulos, J. M. Xu, and M. Moskovits, "Highly-ordered carbon nanotube arrays for electronics applications," *Applied Physics Letters*, vol. 75, pp. 367–369, July 1999.

[99] W. B. Choi, J. U. Chu, K. S. Jeong, E. J. Bae, J.-W. Lee, J.-J. Kim, and J.-O. Lee, "Ultrahigh-density nanotransistors by using selectively grown vertical carbon nanotubes," *Applied Physics Letters*, vol. 79, pp. 3696–3698, Nov. 2001.

[100] W. Cheng, M. Steinhart, U. Gösele, and R. B. Wehrspohn, "Tree-like alumina nanopores generated in a non-steady-state anodization," *J. Mater. Chem.*, vol. 17, no. 33, pp. 3493–3495, 2007.

[101] C. Mu, Y.-X. Yu, R. M. Wang, K. Wu, D. Xu, and G.-L. Guo, "Uniform metal nanotube arrays by multistep template replication and electrodeposition," *Advanced Materials*, vol. 16, no. 17, pp. 1550–1553, 2004.

[102] G. Meng, F. Han, X. Zhao, B. Chen, D. Yang, J. Liu, Q. Xu, M. Kong, X. Zhu, Y. Jung, Y. Yang, Z. Chu, M. Ye, S. Kar, R. Vajtai, and P. Ajayan, "A general synthetic approach to interconnected Nanowire/Nanotube and Nanotube/Nanowire/Nanotube heterojunctions with branched topology," *Angewandte Chemie International Edition*, vol. 48, pp. 7166–7170, Sept. 2009.

[103] Y. Xiang, A. Keilbach, L. Moreno Codinachs, K. Nielsch, G. Abstreiter, A. Fontcuberta i Morral, and T. Bein, "Multiple nanowire species synthesized on a single chip by selectively addressable horizontal nanochannels," *Nano Letters*, vol. 10, pp. 1341–1346, Apr. 2010.

[104] K.-K. Lew, C. Reuther, A. H. Carim, J. M. Redwing, and B. R. Martin, "Template-directed vapor–liquid–solid growth of silicon nanowires," *Journal of Vacuum Science & Technology B: Microelectronics and Nanometer Structures*, vol. 20, no. 1, pp. 389–392, 2002.

[105] K.-K. Lew and J. M. Redwing, "Growth characteristics of silicon nanowires synthesized by vapor-liquid-solid growth in nanoporous alumina templates," *Journal of Crystal Growth*, vol. 254, pp. 14–22, June 2003.

[106] T. E. Bogart, S. Dey, K.-K. Lew, S. Mohney, and J. Redwing, "Diameter-controlled synthesis of silicon nanowires using nanoporous alumina membranes," *Advanced Materials*, vol. 17, no. 1, pp. 114–117, 2005.

[107] I. Lombardi, A. I. Hochbaum, P. Yang, C. Carraro, and R. Maboudian, "Synthesis of high density, size-controlled si nanowire arrays via porous anodic alumina mask," *Chemistry of materials*, vol. 18, no. 4, pp. 988–991.

[108] T. David, D. Buttard, M. D. Hertog, P. Gentile, T. Baron, P. Ferret, and J.-L. Rouvière, "Silicon nanowires grown in nanoporous alumina matrices on oriented silicon substrates investigated by electron microscopy," *Superlattices and Microstructures*, vol. 44, pp. 354–361, Oct. 2008.

[109] X. y. Zhang, L. d. Zhang, G. w. Meng, G. h. Li, N. y. JinPhillipp, and F. Phillipp, "Synthesis of ordered single crystal silicon nanowire arrays," *Advanced Materials*, vol. 13, pp. 1238–1241, Aug. 2001.

[110] B. Marquardt, "Organisation nanometrique de composant (nanotubes de carbone) utilisant des membranes verticales d'alumine anodique poreuse." http://tel.archives-ouvertes.fr/index.php?halsid=pjkpepq00t6oqf5pbns4tj48j3&view_this_doc=pastel-00005877&version=1, Dec. 2009.

[111] X. Yan and Y. Chang, "A thermodynamic analysis of the Cu–Si system," *Journal of Alloys and Compounds*, vol. 308, pp. 221–229, Aug. 2000.

[112] R. U. Nijmegen, "How does an EM work?." http://www.vcbio.science.ru.nl/en/fesem/info/principe/.